Safety First, Bubbles Second: Integrating Regulatory Compliance with Innovation in Rapid Prototyped Focused Ultrasound Devices

Laura Huynh

Thesis submitted to the faculty of the Virginia Polytechnic Institute and State University in partial fulfillment of the requirements for the degree of

Master of Science
In
Biomedical Engineering

Eli Vlaisavljevich,Chair
Adam Maxwell
Shima Shahab

April 25th 2025
Blacksburg, Virginia

Keywords: Histotripsy, Focused Ultrasound, Regulatory Compliance, Risk Mitigation, Rapid Prototyping

Safety First, Bubbles Second: Integrating Regulatory Compliance with Innovation in Rapid Prototyped Focused Ultrasound Devices

Laura Huynh

ABSTRACT

Focused ultrasound (FUS) devices are being developed for noninvasive treatment across a range of clinical applications. High-intensity methods, such as histotripsy, introduce safety and performance considerations that may arise during early stages of prototyping. This thesis presents an evaluation framework intended to support early-stage identification of factors related to clinical and regulatory requirements. The framework was developed using risk management principles to identify risks during prototyping and determine which may be addressed through design modifications for the specific application. For risks not fully mitigated through design, the research focused on three safety domains: biological compatibility (ISO 10993), electrical safety (IEC 60601-1), and acoustic characterization (IEC 62127-1). The framework was applied to a case study involving 3D-printed materials commonly used in rapid prototyping for FUS research, assessing performance according to established guidance documents and international standards. In this context, materials with favorable acoustic performance did not consistently meet biocompatibility criteria, and electrical safety issues were only identifiable through specific testing that might otherwise be overlooked in early development phases. These findings highlight the role of concurrent safety evaluation across multiple areas. Structured assessments during early development produced data aligned with regulatory expectations and identified factors that may influence later design stages. The framework may be applied to full-system prototypes and explored further across various FUS device types.

Safety First, Bubbles Second: Integrating Regulatory Compliance with Innovation in Rapid Prototyped Focused Ultrasound Devices

Laura Huynh

GENERAL AUDIENCE ABSTRACT

This thesis looks at how focused ultrasound (FUS) devices are developed, especially those that use high-intensity energy such as histotripsy. These types of devices are often prototyped without considering safety regulations early in the process. To address this, the research introduces a structured approach to identify potential safety risks. These include how the device materials interact with the body, how safely the electronics operate, and how the ultrasound energy is delivered. The approach uses internationally recognized guidelines to evaluate these areas. A case study was carried out using common 3D-printed materials found in early-stage designs. Tests showed that some materials that worked well for delivering sound energy were not suitable for contact with the body, and certain electrical risks were only found through specific types of testing. These results highlight the importance of checking multiple safety factors at the same time rather than one at a time. The evaluation process helped identify safety-related issues early in development and provided information that could support future design decisions. This approach may be applied to other ultrasound technologies and expanded to full devices as development continues.

DEDICATION

I would like to dedicate this work to my beautiful mother. I've learned a lot from this work, but even more from you. Thank you for sacrificing so much for me, even when things weren't easy.

ACKNOWLEDGEMENTS

I am not sure why I listened to you Sarah Hall about doing a thesis, I have never lost so much sleep in my life, but it was all worth it.

First and foremost, thank you to my advisor Eli Vlaisavljevich who gave me a chance to join the lab as a sophomore. Your mentorship and guidance throughout this journey have been invaluable, and I am grateful for the opportunities you've provided me to grow as a researcher and engineer. I would also like to express my deep appreciation to my other advisor, Adam Maxwell, for his consistent support and expertise. I don't know how, but it seems like you know everything. Your technical insights and thoughtful feedback significantly helped me with this research and helped me navigate the most challenging aspects of this project, which was finding and reading all the guidance documents and standards.

Special thanks to Sarah Hall, the person I simultaneously want to thank and blame for this entire experience. When you suggested I do a thesis, you conveniently left out the part about coming into lab on weekends and forgetting what daylight looks like. However, your mentorship and support through not only senior design but these past few years have been a tremendous source of guidance and encouragement. You've helped me navigate the most challenging moments with humor, insight, and endless patience, and for that, I am truly grateful.

And to Jess, who witnessed my full range of thesis-induced emotions, from the high fives when experiments worked to the crashing out when they didn't. To my other half of double trouble, thank you for being there for every celebration and every meltdown, always ready with a listening ear, a joke to lighten the mood, or a Chipotle to keep me going. Your friendship made the long hours and stressful moments so much more bearable.

And to the rest of my lab members, my sincere thanks for creating an environment where both scientific breakthroughs and breakdowns were equally supported. Sara, thank you for helping me figure out how to calculate all the different intensities and getting the trigger to work. I don't know what I would have done without you. Lexi thank you for being you and listening to my problems when you come into lab and trying to help me troubleshoot. Let me know when you are hiring, I might be interested. Victor, thank you for all your help over the years! You are always willing to lend a hand even during your busiest moments. Thank you, Ruth, for letting me use the "Chernobyl table" even when you had it booked, sorry for the occasional hijacking of equipment! Your generosity and flexibility saved me countless times. Special thanks to Moon for helping me build all those single elements. I am truly appreciative all your help, I genuinely don't think I would have finished my thesis without you. To everyone else I did not mention by name, I am very thankful to have gotten to know each and every one of you. This lab has been more than just a workplace, it's been a community that made this challenging journey not just possible, but sometimes even fun.

And lastly, to my friends and family who wondered why I don't call or text them as often. Thank you for your unconditional support, for pretending to understand what I was talking about when I excitedly explained my research. To my friends who checked in on me even when I disappeared for weeks at a time, your love and encouragement were the foundation that made this work possible. To my mom, thank you for believing in me even when I doubted myself, and for celebrating every small victory along the way.

Table of Contents

Chapter 1. Introduction *1*

1.1 Background on Focused Ultrasound **1**

1.2 Fabrication of FUS Transducers **2**

1.3 Challenges in Prototype Design for Clinical Readiness **10**

1.4 Outline of Thesis **12**

Chapter 2: Regulatory Guidelines and Considerations *20*

2.1 Introduction to Regulatory Requirements for Medical Devices **20**

2.2 Risk Management **21**

2.3 Design Controls **26**

2.4 International and Industry Standards **28**

2.4.1 ISO 10993: Biocompatibility of Medical Devices 29

2.4.2 IEC 60601-1: Basic Safety and Essential Performance of Medical Electrical Equipment 33

2.4.3 IEC: Acoustic characterization 38

Chapter 3: Safety and Effectiveness Evaluation on Rapid Prototyped Histotripsy Single Element Transducer for Endoscopic Use *43*

3.1 Introduction **43**

3.2 Methods **45**

3.2.1 Material Properties Testing 45

3.2.2 ISO 10993 Biocompatibility: Cytotoxicity Test 48

3.2.3 IEC 60601-1 Electrical Safety Testing 50

3.2.4 Single Element Construction 57

3.2.5 IEC 62127-1: Acoustic Characterization 58

3.3 Results **62**

3.3.1 Acoustic Properties of 3D-Printed Resins 62

3.3.2 ISO 10993 biocompatibility: Cytotoxicity Test Results 64

3.3.3 Electrical Safety Test Results 66

3.3.4 Acoustic Characterization 68

3.4 Discussion **75**

3.5 Conclusions and Future Work **77**

3.7 References **79**

Chapter 4: Conclusions and Future Directions ***81***

Appendix A. Example of Risk Assessment For FUS Devices ***83***

Appendix B. Acoustic Impedance and Sound Speed Matlab Code ***86***

Appendix C. Attenuation Matlab Code ***88***

Appendix D. Electrical Safety Analyzer Parameters ***91***

Appendix E. I_{SPTA} and I_{SPPA} Matlab Code ***92***

List of Figures

Figure 1-1. Illustration of the key components of FUS transducer element. High electrical voltage is applied to the piezoelectric disc which causes it to vibrate and generate ultrasound waves, which then travel through the matching layer, lens, and coupling medium before reaching the treatment medium at the focus. 4

Figure 1-2. Photograph of an in-house designed amplifier box, featuring a 3 MHz element connected via coaxial wiring to one of the channels. The system supports up to 32 channels and includes a green motherboard with an FPGA for controlling pulse timing and intensity, along with yellow pulser cards that amplify electrical signals to drive piezoelectric elements. 7

Figure 1-3. Spatial configurations of FUS transducers. (a) Single-element concave transducer with a fixed focal point. (b) Annular array with concentric ring elements for adjustable depth. (c) Multi-element array arranged along a spherical or elliptical surface for dynamic focusing across a larger volume..... 8

Figure 2-1. An overview of the key steps in risk management according to ISO 14971, including risk analysis, risk evaluation, risk control, evaluation of overall residual risk, risk management review, and production and post-production activities. 22

Figure 2-2. This figure illustrates the systematic flow of design controls with risk management integration throughout the medical device development process. The flow chart demonstrates how risk management activities inform and interact with each phase of design controls, ensuring that potential hazards are identified early and mitigated effectively before product release. 27

Figure 3-1. All 3D-printed material candidates tested for their material properties. 46

Figure 3-2. Experimental setup for material properties testing. A 3 MHz single-element transducer and a high-sensitivity rod hydrophone were mounted on a positioning system in degassed,

deionized water. Acoustic signals were recorded via a digital oscilloscope and converted into pressure values (MPa) using MATLAB. The hydrophone was first positioned at the acoustic focus (75 mm) and then moved axially to the far field approximately 120 mm beyond the focus, resulting in a total distance of 195 mm from the transducer. 47

Figure 3-3. The workflow for cytotoxicity testing includes extraction of 3D-printed materials, application of extracts to L929 cells, microscopic observation, and assessment of cell viability using the MTT assay and microplate reader. 48

Figure 3-4. This figure illustrates the ground bond test procedure where the ESA supplies power to the amplifier (DUT), causing current to flow through the protective earth conductor of the DUT The return current passes through the conductive parts of the DUT (metal screws) and returns via the return lead to the ESA, which measures the resistance of the protective earth path to ensure it meets safety standards..... 51

Figure 3-5. Adapted from "3 Ways to Simplify Medical Device Testing," HIK Consulting [6]. Ground bond test configuration measuring continuity between the power plug ground pin and the device chassis..... 51

Figure 3-6. Earth leakage test schematic showing how the analyzer applies current to the DUT and measures leakage through the ground path to the device chassis. 52

Figure 3-7. This figure illustrates the Earth Leakage Test procedure, where the ESA supplies power to the amplifier (DUT) through a variable transformer to enable testing at 110% of the rated voltage, as required by IEC 60601-1 [4]. Current flows through the DUT, and the return current passes through the MD, which simulates human body impedance. The ESA then measures any leakage current flowing through the protective earth, ensuring compliance with test limits of ≤ 5 mA (NC) and ≤10 mA (SFC) [4]. 52

Figure 3-8. Single-touch enclosure leakage current test schematic illustrating how the analyzer simulates a single fault condition and measures current flowing from the device enclosure to ground through a simulated patient or operator touch. 53

Figure 3-9. This figure illustrates the test setup for measuring single-touch enclosure leakage current. The ESA supplies power to the amplifier (DUT) through a variable transformer, which allows testing at 110% of the rated voltage as required by IEC 60601-1 [4]. Current flows through the DUT, with any leakage current returning through the high probe and passing through the MD, which simulates human body resistance. The ESA then measures the current leaking through the enclosure to ensure compliance with limits of ≤100 µA (NC) and ≤ 500 µA (SFC) [4]. 54

Figure 3-10. Two-touch enclosure leakage test schematic showing current measurement between two simultaneously accessible conductive parts, simulating a potential path through a patient or operator under a fault condition. 55

Figure 3-11. This schematic demonstrates the test setup for measuring two-touch enclosure leakage current. The ESA supplies power to the amplifier (DUT) through a variable transformer, enabling testing at 110% of the rated voltage [4]. As current flows through the device, any leakage current from the enclosure is detected as it flows from Probe Hi to Probe Lo, passing through the MD, which simulates human body impedance. The ESA then measures the leakage current to ensure compliance with IEC 60601-1 limits of ≤100 µA under normal conditions (NC) and ≤500 µA under single-fault conditions (SFC) [4]. 55

Figure 3-12. Patient leakage current test schematic showing how current is measured from the applied parts through the simulated patient pathway to ground, assessing leakage under normal and single fault conditions. 57

Figure 3-13. This figure illustrates the test setup for measuring patient leakage current. The ESA, powered through the variable transformer, supplies power to the amplifier (DUT), and current flows from the transducer through the 0.9% saline water to the copper tape, which acts as a conductive path. Return current flows from Probe Hi through the MD. The ESA then checks for any current leaking through the transducer, ensuring compliance limits of ≤100μA during NC and ≤500μA under SFC [4]..... 57

Figure 3-14. Experimental setup for grid scanning of the acoustic field using a 3 MHz single-element transducer and a high-sensitivity hydrophone..... 59

Figure 3-15. A representative pressure waveform used to calculate pulse duration. The time points where the squared pressure waveform reaches 10% (green) and 90% (red) of its total energy are marked, and the interval between them is used to determine the pulse duration..... 60

Figure 3-16: The red shaded area highlights the part of the pulse (i.e. the pulse duration) used to calculate pulse average intensity. The red dashed line marks the peak of this average intensity across all grid points, which is reported as I_{SPPA}..... 61

Figure 3-17. Acoustic material properties including acoustic impedance (MRayl), sound speed (m/s), and attenuation coefficient (dB/cm) calculated using MATLAB. Results are presented for each 3D-printed resin candidate..... 63

Figure 3-18. Cell morphology images taken following 24h extract exposure to 3D-printed materials. Cells were visually assessed for signs of cytotoxicity, such as cell rounding, detachment, or lysis. Images include negative control (untreated), positive control (cytotoxic agent), and each test material. Images captured at 40x magnification. 65

Figure 3-19. Bar graph showing percentage of cell viability for 3D-printed materials under 24-hour (left) and 72-hour extract (right) conditions. The MTT assay was performed in accordance with ISO 10993-5, with 70% viability used as the cytotoxicity threshold. 66

Figure 3-20. Measured pressure waveforms of biocompatible 3D printed resins and PerFORM as a control. 69

Figure 3-21. Pressure waveform grid scan of different materials acquired over a 5.5 x 5.5 mm grid in the yz-plan using a step size of 0.25 mm at the focus. The color bar indicates peak pressure values where red represents the highest peak pressure and blue represents the lowest peak pressure. 70

Figure 3-22. The red shaded area represents the pulse duration over which I_{SPPA} values were integrated. I_{SPPA} values are indicated by the gray dashed line for each of the four tested resins.. 71

Figure 3-23. The red shaded area represents the pulse duration over which I_{SPPA} values were integrated. I_{SPPA} values for each material after scaling pressure waveforms to a peak negative pressure of -30 MPa are indicated by the gray dashed line for each of the four tested resins. 72

Figure 3-24. Lateral (top) and elevational (bottom) beam profiles for PerFORM and Surgical Guide. Beam widths were measured at the FWHM of the peak negative pressure and are indicated by red horizontal bars. 73

Figure 3-25. Lateral (top) and elevational (bottom) beam profiles for Biomed White and Biomed Elastic 50A. Beam widths were measured at the FWHM of the peak negative pressure and are indicated by red horizontal bars. 74

List of Tables

Table 1: Severity Levels for Risk Analysis 23

Table 2: Occurrence Levels for Risk Analysis 23

Table 3: Risk assessment matrix showing the relationship between severity and occurrence levels. This matrix provides a framework for evaluating and prioritizing risks based on the level, where high risk rating (red) is an unacceptable risk, medium risk (orange) is an important risk, and low risk (green) is an acceptable risk 23

Table 4. Risk assessment for a rapid-prototyped histotripsy transducer intended for endoscopic use. Risks were identified across thermal, electrical, mechanical, biological, chemical, acoustic, and user-related domains. Each risk was rated before and after proposed design mitigations based on a structured risk analysis framework following ISO 14971. 26

Table 5: Adapted from ISO 10993-1:2009 [10] showing potential biological evaluation tests based on the nature of body contact and duration of exposure. Categories include surface, external communicating, and implant devices, with exposure durations classified as limited (<24 h), prolonged (24 h–30 days), and permanent (>30 days). Crosses indicate biological endpoints that may require evaluation depending on risk analysis. Additional testing is not needed if existing data sufficiently address the biological safety endpoints. 31

Table 6: Summary of electrical safety tests for FUS devices, indicating the specific risks mitigated by each test and their relevance to device development and safety. 37

Table 7. Summary of acoustic characterization tests for FUS devices, indicating the specific risks mitigated by each test and their relevance to device development and safety. 40

Table 8: Health risks and corresponding mitigation measures for FUS devices 43

Table 9: Design Controls Traceability Matrix- Translation of User Needs into Design Requirements, Outputs, and Verification Methods in Accordance with International Standards (ISO 10993, IEC 60601-1, IEC 60601-2-62, and IEC 62127-1). 44

Table 10: Mean ± standard deviation of acoustic material properties for candidate 3D-printed resins, including acoustic impedance (MRayl), sound speed (m/s), and attenuation coefficient (dB/cm). 64

Table 11: Qualitative morphological grading scale for cytotoxicity evaluation of extracts, as defined by ISO 10993-5. Grading is based on the percentage of cell damage or detachment observed microscopically, with scores ranging from 0 (no reactivity) to 4 (severe reactivity). ... 65

Table 12: Summary of ground bond test measurements across multiple DUT contact points. The table includes measured resistance values, the specified safety limit, and pass/fail evaluation based on compliance with IEC 60601-1 standards. 67

Table 13: Summary of Leakage Test Results Under Normal Conditions (NC) and Single Fault Conditions (SFC). The table presents the measured values taken from the OMNIA II 8206 Electrical Safety Analyzer for each test type alongside their respective limits for both conditions, with pass/fail status indicated for each measurement. 67

Table 14: Summary of peak positive and peak negative pressures, along with acoustic intensity values computed from pressure waveform data across 2025 spatial points at the acoustic focus. 75

Chapter 1. Introduction

1.1 Background on Focused Ultrasound

Pursuing less invasive cancer therapies has driven the development of innovative technologies because they offer significant advantages over open surgery. These benefits include reduced blood loss, fewer complications, quicker recovery times, and a lower risk of infection [1]. As a result, there has been a growing shift toward techniques that minimize surgical trauma while maintaining therapeutic effectiveness. Among these, focused ultrasound (FUS) has emerged as a promising modality, utilizing precise acoustic energy to target and treat tissues within the body without the need for incisions [2]. By concentrating ultrasound waves into a small focal point, this technology can achieve localized effects, such as heating or mechanical disruption, depending on the intensity and parameters of the ultrasound waves. These effects enable a wide range of medical applications, from tissue ablation to neuromodulation, making FUS a versatile tool in modern medicine.

FUS operates through two primary mechanisms: thermal and mechanical effects. High-intensity focused ultrasound (HIFU) primarily relies on thermal effects for tissue treatment. HIFU heats the targeted tissue to high temperatures, causing tissue necrosis and effectively destroying the diseased tissue through the application of continuous or pulsed ultrasound at moderate intensity or pressure. This pressure is often describes using peak negative pressure (p-) which is the lowest pressure reached in the wave cycle where the tissue is being pulled apart rather than compressed. At moderate levels (p- ~ 5-10 MPa), thermal effects dominate, enabling controlled heating without strong mechanical effects like cavitation [3]. While HIFU relies on thermal effects, histotripsy is a type of HIFU that uses mechanical effects to break down tissue. This process is achieved through short, high-amplitude ultrasound pulses (p- ~ 25-30 MPa) that induce the formation of a cavitation

bubble cloud [4]. The rapid expansion and collapse of these bubbles generate intense, localized mechanical strain, effectively fractionating targeted cells into acellular debris [4]. Beyond tissue ablation, low-intensity focused ultrasound (LIFU) refers to applications that use acoustic intensities and pressures comparable to those in diagnostic imaging. Diagnostic ultrasound is governed by FDA-defined limits that are specifically intended to avoid causing any bioeffects. In contrast, LIFU operates within those same safety ranges but leverages focused energy and specific pulsing strategies to intentionally produce reversible bioeffects, such as the stimulation or suppression of neural activity. This allows LIFU to non-invasively modulate brain function while remaining within the established safety parameters [5].

1.2 Fabrication of FUS Transducers

Developing a FUS transducer involves several considerations that influence performance, safety, and clinical use. The main components of a transducer including multiple layers of different materials, and may include piezoelectric material, backing layers, matching layers, lenses, and a housing [6]. Each part contributes to acoustic output and functionality. Material selection influences factors such as compatibility with tissue, structural performance, and how effectively acoustic energy is delivered [7]. Factors such as device geometry, operating frequency, and beam steering or focusing capabilities all play a role in how effectively acoustic energy reaches the intended treatment site [7]. Fabrication methods are selected to balance precision, repeatability, and efficiency, particularly during iterative design and prototyping stages.

The piezoelectric elements are the core of a FUS transducer. The elements are responsible for converting electrical energy into mechanical vibrations, enabling the generation of ultrasound waves. This component is typically made from piezoelectric materials like lead-zirconate-titanate (PZT). Examples explored in previous studies include PZT-5A/epoxy composites and other

specific formulations of PZT such as PZ39 and PZ54 (CTS Denmark A/S, Kvistgård, Denmark), among other formulations aimed at improving the efficiency of converting electrical energy into acoustic pressure [8]. Each piezoelectric element has a resonant frequency at which it operates most efficiently, enabling optimal energy conversion with minimal loss [9]. However, piezoceramic elements are usually efficient over a range of frequencies bounded by their mechanical and electrical resonances. Operating near resonance enhances both output amplitude and control over the acoustic signal.

In many transducers, a backing layer is used to absorb unwanted acoustic waves and help manage vibration and device stability [10],[11]. However, in high-intensity focused ultrasound (HIFU), maximizing acoustic output efficiency is critical. Any energy absorbed by the backing is lost as heat rather than being transmitted to the target [12]. High-intensity transducers, such as those used in HIFU or histotripsy, may use air-backing or other materials to direct more energy forward and minimize internal losses [13]. Similarly, the transition of sound waves from the piezoelectric element into tissue presents another challenge due to differences in acoustic impedance [12]. Piezoelectric materials like PZT have high impedance, while soft tissue or water has much lower impedance, leading to energy loss at the boundary [14]. Matching layers can help reduce energy loss by improving acoustic transmission between materials with different properties [15]. These layers are typically placed in front of the piezoelectric element with a thickness of one-quarter wavelength ($\lambda/4$) to optimize transmission [15]. The inclusion of matching or backing layers depends on the application's requirements for focus, intensity, and thermal performance. Although these layers are commonly used to improve energy coupling and bandwidth, they are not always necessary. Some high-intensity applications such as histotripsy or certain HIFU designs intentionally omit them to reduce internal heat buildup and maximize peak pressure output [16].

In other cases, simplicity, miniaturization, or fabrication constraints may also justify their exclusion. Furthermore, some transducers include a lens to shape or focus the beam, depending on whether precise targeting is required. Lastly, the housing surrounds the transducer assembly, providing protection, structural support, and a barrier to external environmental conditions. Together, these components form the basic transducer construction illustrated in **Error! Reference source not found.**.

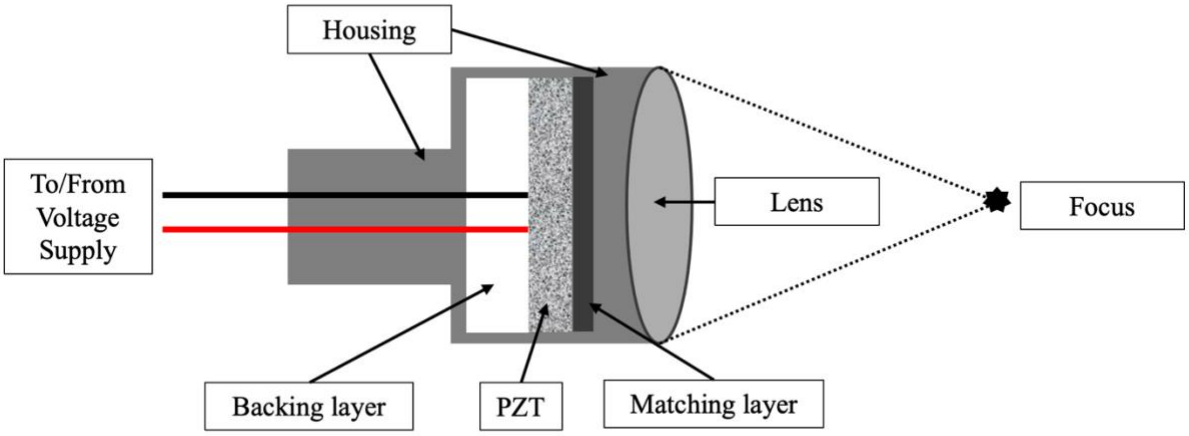

Figure 0-1. Illustration of the key components of FUS transducer element. High electrical voltage is applied to the piezoelectric disc which causes it to vibrate and generate ultrasound waves, which then travel through the matching layer, lens, and coupling medium before reaching the treatment medium at the focus.

While the basic construction shown in **Error! Reference source not found.** outlines the key components of a focused ultrasound transducer, the performance and safety of the device also depend on the materials selected for those components, particularly the housing and lens. These outer structures interface directly with the external environment and should be chosen not only for their ability to support acoustic wave transmission, but also for their structural, biological, electrical, and thermal reliability during operation.

From an acoustic perspective, the housing and lens materials should have impedance values that fall between those of the internal transducer piezoelectric element and the external medium,

such as water or tissue [17]. This reduces reflection at material boundaries and helps preserve the intensity of the ultrasound beam as it exits the device. Additionally, materials with low attenuation minimize the absorption and scattering of acoustic energy, allowing more of the transmitted wave to reach the target region [18]. While increasing drive power may seem like a way to offset attenuation, it introduces additional heat and electrical load, which can lead to material degradation, insulation failure, or operation beyond safe limits.

Beyond acoustic considerations, the materials used for the housing and lens may be selected based on electrical, thermal, geometric, biocompatibility, and mechanical characteristics relevant to device function. Electrical insulation is included to limit leakage currents that can occur in systems operating at high voltages [19]. Thermal conditions during device operation, particularly under prolonged activation or high-intensity pulsing, can result in elevated surface temperatures at the transducer, which may exceed safety limits and pose risks to surrounding tissue [20],[21],[22]. The geometry of the lens can influence the shape and location of the acoustic focus, and variations in this geometry may cause focal shifts or reduce beam uniformity [23]. Biocompatibility is assessed for components that contact the patient using standardized methods that evaluate whether a material induces unwanted biological responses [24]. Mechanical behavior under conditions such as handling, transportation, cleaning, and reuse may also be considered, as fracture or degradation of the housing or lens can expose internal components or impair acoustic performance [19]. These electrical, thermal, geometric, biological, and mechanical characteristics, along with acoustic properties, contribute to overall device performance during clinical use.

FUS devices rely on electrical systems to generate the signals that drive the ultrasound transducer. These systems typically include a signal generator, which sets the frequency and waveform pattern [25]. The signal is applied to the transducer's piezoelectric element, causing it

to vibrate and emit focused ultrasound waves. Depending on the application, an amplifier may be used to increase the signal's strength to achieve the desired therapeutic effect. Different applications use different setups. High-intensity applications like tissue ablation or histotripsy require high-power of energy and therefore rely on significant amplification [8], [26]. In contrast, lower-intensity applications such as neuromodulation may require less amplification or may not use an amplifier at all, depending on the power and duration of the signal [27]. Furthermore, some devices use a single transducer element, while others use arrays composed of many elements. These arrays allow the ultrasound beam to be electronically steered or shaped by adjusting the timing of signals sent to each element, which requires precise control through specialized electronics designed to manage timing and reduce system complexity [28]. An example from our lab is shown in **Error! Reference source not found.**. In this system, a field-programmable gate array (FPGA) acts as the pulse generator and controls the timing and intensity of signals sent to each transducer channel [29]. These signals are routed to a bank of high voltage pulsers housed within an amplifier box, which amplify the signals to the levels required for histotripsy. The high-voltage driver operates by cyclically charging and discharging current through an inductor in parallel with the transducer, creating the short, high-voltage pulses needed to generate cavitation.

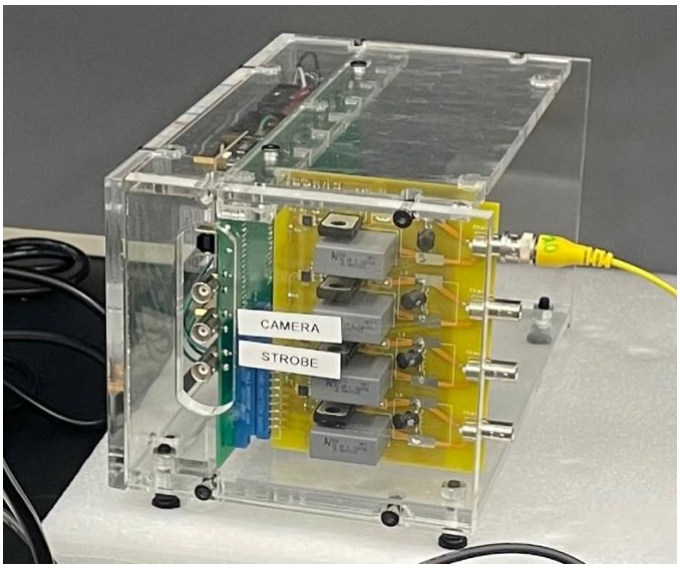

Figure 0-2. Photograph of an in-house designed amplifier box, featuring a 3 MHz element connected via coaxial wiring to one of the channels. The system supports up to 32 channels and includes a green motherboard with an FPGA for controlling pulse timing and intensity, along with yellow pulser cards that amplify electrical signals to drive piezoelectric elements.

The spatial configuration or geometry of a FUS transducer can be modified to suit the application. A common design in FUS systems is the single-element concave transducer, which focuses ultrasound waves at a fixed point (Figure **0-3.**a) [30]. The focal region is shaped by geometric factors such as curvature and aperture size, which define the f number as the ratio of focal length to aperture diameter [31]. While single-element transducers can achieve strong focusing, including at large apertures, practical limits may arise from the fabrication process [32]. For example, 3D printing can restrict achievable f numbers due to constraints in curvature, resolution, or build size, which can influence the range of transducer geometries that are feasible [32]. Although the focus of a single-element transducer is fixed, it can be adjusted between uses by modifying the geometry or incorporating acoustic lenses. Some systems use multi-element transducers, such as phased arrays, which consist of multiple piezoelectric elements arranged in defined patterns to enable electronic control of beam shape and direction [7]. One example of a multi-element configuration is an annular array (shown in Figure **0-3.**b), where elements are

arranged in concentric rings [30]. Another example is elements arranged and placed along the curved surface of a sphere or ellipse (Figure **0-3.**c) [30]. By adjusting the timing of signals sent to each element, these arrays can electronically shape or steer the ultrasound beam [7]. This enables real-time control of focus and direction without moving the transducer, offering advantages in complex procedures that require precision and adaptability [7].

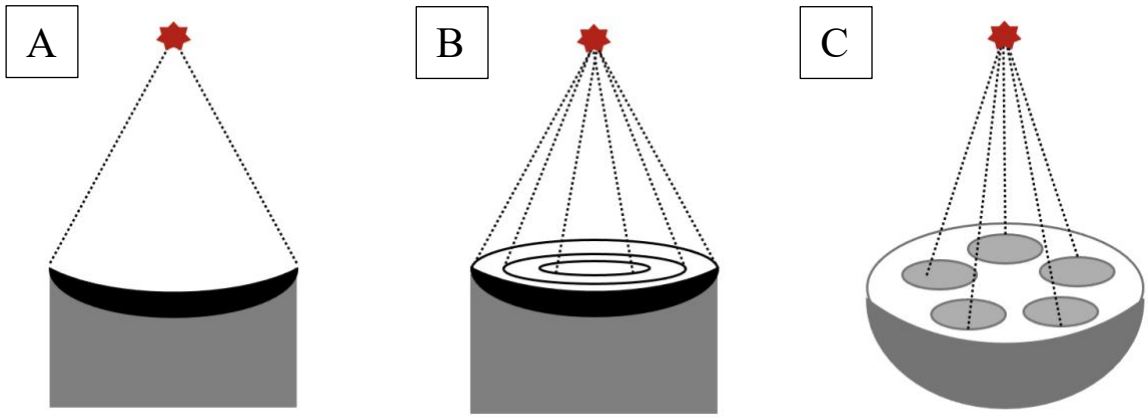

Figure 0-3. Spatial configurations of FUS transducers. (a) Single-element concave transducer with a fixed focal point. (b) Annular array with concentric ring elements for adjustable depth. (c) Multi-element array arranged along a spherical or elliptical surface for dynamic focusing across a larger volume.

Specialty transducer manufacturing companies often supply many of the FUS transducers used in research and clinical applications [32]. However, given the need for customization to meet specific applications, such as integrating imaging feedback probes, generating complex focal patterns, or maximizing the use of available acoustic windows in the body, standard commercial options may not meet the specific design constraints or integration needs of all applications [32]. To address this, rapid prototyping methods have been explored as a solution in developing main components, specifically the housing/lens of the transducer [33], [34]. At the moment, most FUS components in research are 3D printed using stereolithography (SLA) in house or selective laser sintering (SLS) acquired by third-party manufacturers [33], [34]. SLA uses a laser to cure liquid

resin layer by layer, producing high-resolution parts with smooth surfaces, while SLS uses a laser to fuse powdered material, creating durable components with complex geometries [35]. Although injection molding for FUS components has been explored in previous studies [33], [34], these methods are better suited for mass production once the transducer design has been finalized and validated. Injection molding excels at producing durable, high-precision parts at scale and has an extensive material list, but it requires costly, time-intensive tooling and machine startup, making it impractical for iterative design and prototyping. In contrast, 3D printing is particularly valuable in research and development, as it allows engineers to quickly prototype, test and refine transducer designs to meet specific performance criteria without the high costs [32]. However, a common limitation of 3D printing is the limited selection of materials, along with the lack of complete material characterization compared to traditional manufacturing methods such as injection molding or CNC machining [33], [34].

Not all materials with specific acoustic, mechanical, thermal, or electrical properties are compatible with 3D printing, which means the material properties of printed parts, such as impedance and attenuation, may not always match those of traditionally manufactured components [32]. Additionally, speed and scalability are further limitations, as 3D printing can be very slow for large or highly detailed parts [31-33]. Since 3D-printed components are relatively new in clinical device development, additional testing may be needed to meet regulatory expectations [36]. This makes it challenging to compare them to predicate devices as they serve as benchmarks for safety and efficacy in regulatory approval processes. This lack of established precedent for 3D-printed devices in clinical applications introduces additional hurdles in demonstrating compliance with regulatory standards, such as biocompatibility and quality assurance. As a result, extensive testing and validation are often required in FUS devices for them to advance into clinical

applications, increasing both development time and costs. Although not exhaustive, this thesis outlines the critical testing needed for rapid prototyped FUS devices to meet regulatory standards, based on a risk analysis. The risk-based framework is used to identify potential hazards and determine which tests are necessary. While not all tests were experimentally performed, each is discussed and justified based on the level of risk. In some cases, risks can be reduced or addressed through design decisions, limiting the need for certain tests during early-stage development.

1.3 Challenges in Prototype Design for Clinical Readiness

Despite the broad applications of FUS, translating the research to clinical use faces several challenges. As an emerging technology, one significant hurdle is the lack of regulatory guidelines into the design and development of FUS devices. This subchapter provides an overview of the IDE process and its significance in medical device development. While efforts have been made to better understand the interactions between FUS-induced bioeffects and biological tissues, these advancements have not always been accompanied by parallel progress in regulatory standardization [37]. In academic environments, research often prioritizes innovation and proof-of-concept studies, which are critical for pushing the boundaries of the technology. However, this focus can come at the expense of addressing the regulatory considerations necessary for clinical translation. For example, in the development of histotripsy transducers, academic research may focus heavily on understanding the physics behind bubble cloud formation [38], optimizing cavitation thresholds [37], and ablation precision to improve treatment efficacy [39], all of which are agnostic to the details of the device itself. While these advancements are essential in improving the technology, they are not always accompanied by thorough documentation of safety parameters, electrical safety testing, or biocompatibility assessments, all of which are key components required to meet regulatory standards. As a result, early-stage FUS prototypes may lack the necessary

documentation and performance validation to demonstrate that the devices are safe for human testing. This oversight can create significant delays when transitioning promising technologies from the laboratory to patients who could benefit from them [40]. To bridge this gap between innovation and regulations, there is a need for a proactive approach that integrates regulatory considerations into the early stages of FUS device development in academic research. By doing so, we can ensure that FUS technologies are not only innovative but also safe, reproducible, and ready for clinical use.

A component of clinical translation and testing for a new device is obtaining an investigational device exception (IDE). An IDE is an approval from the U.S. Food and Drug Administration (FDA) that allows a medical device to be used in clinical trials to gather safety and effectiveness data before seeking full market approval [41]. In other words, it permits the testing of a medical device on humans, even though it has not yet received FDA clearance or approval for general use. According to the FDA, an IDE submission must include a comprehensive investigational plan, detailing the study objectives, device description, and methodology for evaluating safety and performance [42]. In addition, developers must provide adequate justification for preclinical testing data**,** and risk analysis documentation**,** outlining potential hazards and mitigation strategies to ensure patient safety [42]. However, the requirements for an IDE submission and the involvement of the FDA depend on the risk classification of the device study: significant risk (SR) and nonsignificant (NSR). Under 21 CFR 812.3(m), a SR device is one that could present serious risks to a subject’s health, safety, or welfare [43]. This includes devices intended as implants, those used to support or sustain human life, or those crucial for diagnosing, treating, or preventing disease, all of which carry potential for serious harm. Essentially, any device that could significantly impact a subject's well-being falls under the significant risk

classification. Therefore, SR devices require a full IDE submission and approval by the FDA before clinical trials can begin. On the other hand, a NSR device is one that does not fit any of the definitions for a SR device meaning it is deemed not to pose a serious risk to patients and as a result may only require an abbreviated IDE. In such cases, the clinical study can proceed under Institutional Review Board (IRB) approval alone, without FDA approval. Yet, the FDA may become involved in some circumstances including if the IRB is uncertain about the risk determination or if the FDA disagrees with the IRB's NSR determination [43]. Lastly, for legally marketed devices that are already FDA-approved, an IDE is generally not required if the device is used according to its approved labeling and intended purpose. However, if the device is being studied for a new indication or in a different population, an IDE may still be necessary if the device's use or design increases in risk to patients. For histotripsy transducers, the full IDE submission would be typically required due to their higher risk to the patient and the novel nature of the technology, whereas a LIFU transducer may only require an abbreviated IDE since it operates at lower energy levels, posing less risk the patient. This thesis will explore how to meet the regulatory requirements for this process through risk management and design controls ensuring a smooth transition from prototype to clinical evaluation.

1.4 Outline of Thesis

The goal of this thesis is to propose a framework that outlines a development process aligned with regulatory expectations. This framework aims to streamline FUS innovations from research into clinical trials and market readiness by examining current FUS transducer prototyping methods and demonstrating how tools like risk management and design controls help integrate safety and regulatory requirements at every stage of development, from concept to IDE

submission. Chapter 1 examined the key aspects of FUS transducer fabrication, including material selection, design considerations, and manufacturing techniques.

Chapter 2 expands on the specific regulatory standards and considerations that govern FUS device development, providing a comprehensive overview of the regulatory landscape. This chapter details risk management methodologies, design control processes, and international standards that are essential for bringing FUS devices to market. Particular attention is given to biocompatibility requirements, electrical safety standards, and acoustic characterization protocols that are critical for ensuring patient safety and device efficacy.

Chapter 3 applies key regulatory concepts to specific case studies of FUS transducers, focusing on a rapid-prototyped histotripsy single element device. Through evaluation of material properties, biocompatibility testing, electrical safety, and acoustic characterization, this chapter demonstrates how regulatory requirements can inform early-stage design and testing. The results offer insight into the performance and safety of 3D-printed components in FUS applications, establishing a foundation for regulatory-aligned prototype development.

Chapter 4 concludes this thesis by combining key findings and offering a structured approach to regulatory-compliant FUS device development. This chapter presents recommendations for researchers and developers navigating the transition from laboratory prototypes to clinically viable devices, highlighting strategies for addressing regulatory challenges while maintaining innovation. The framework presented offers a roadmap for future FUS technology development that balances regulatory compliance with technological advancement, potentially accelerating the clinical translation of promising FUS therapies for patient benefit.

References

[1] K. Mohiuddin and S. J. Swanson, “Maximizing the benefit of minimally invasive surgery,” *J. Surg. Oncol.*, vol. 108, no. 5, pp. 315–319, Oct. 2013, doi: 10.1002/jso.23398.

[2] O. Al-Bataineh, J. Jenne, and P. Huber, “Clinical and future applications of high intensity focused ultrasound in cancer,” *Cancer Treat. Rev.*, vol. 38, no. 5, pp. 346–353, Aug. 2012, doi: 10.1016/j.ctrv.2011.08.004.

[3] Gail Ter Haar and C. Coussios, “High intensity focused ultrasound: Physical principles and devices,” *Int. J. Hyperthermia*, vol. 23, no. 2, pp. 89–104, Jan. 2007, doi: 10.1080/02656730601186138.

[4] Z. Xu, T. L. Hall, E. Vlaisavljevich, and F. T. Lee, “Histotripsy: the first noninvasive, non-ionizing, non-thermal ablation technique based on ultrasound,” *Int. J. Hyperth. Off. J. Eur. Soc. Hyperthermic Oncol. North Am. Hyperth. Group*, vol. 38, no. 1, pp. 561–575, 2021, doi: 10.1080/02656736.2021.1905189.

[5] H. Baek, K. J. Pahk, and H. Kim, “A review of low-intensity focused ultrasound for neuromodulation,” *Biomed. Eng. Lett.*, vol. 7, no. 2, pp. 135–142, May 2017, doi: 10.1007/s13534-016-0007-y.

[6] M. Genovese, “Ultrasound Transducers,” *J. Diagn. Med. Sonogr.*, vol. 32, no. 1, pp. 48–53, Jan. 2016, doi: 10.1177/8756479315618207.

[7] R. P. Williams, J. C. Simon, V. A. Khokhlova, O. A. Sapozhnikov, and T. D. Khokhlova, “The histotripsy spectrum: differences and similarities in techniques and instrumentation,” *Int. J. Hyperthermia*, vol. 40, no. 1, p. 2233720, Dec. 2023, doi: 10.1080/02656736.2023.2233720.

[8] C. Adams, T. M. Carpenter, D. Cowell, S. Freear, and J. R. McLaughlan, “HIFU Drive System Miniaturization Using Harmonic Reduced Pulsewidth Modulation,” *IEEE Trans. Ultrason.*

Ferroelectr. Freq. Control, vol. 65, no. 12, pp. 2407–2417, Dec. 2018, doi: 10.1109/TUFFC.2018.2878464.

[9] J. Liu, Y. Lu, Z. Wang, S. Li, and Y. Wu, "Three Frequency Up-Converting Piezoelectric Energy Harvesters Caused by Internal Resonance Mechanism: A Narrative Review," *Micromachines*, vol. 13, no. 2, p. 210, Jan. 2022, doi: 10.3390/mi13020210.

[10] C. Hou *et al.*, "Optimized Backing Layers Design for High Frequency Broad Bandwidth Ultrasonic Transducer," *IEEE Trans. Biomed. Eng.*, vol. 69, no. 1, pp. 475–481, Jan. 2022, doi: 10.1109/TBME.2021.3098567.

[11] H. Kim, J. Yoo, D. Heo, Y.-S. Seo, H. G. Lim, and H. H. Kim, "High-Attenuation Backing Layer for Miniaturized Ultrasound Imaging Transducer," *IEEE Trans. Ultrason. Ferroelectr. Freq. Control*, vol. 69, no. 6, pp. 1960–1969, Jun. 2022, doi: 10.1109/TUFFC.2022.3164451.

[12] C. Hou *et al.*, "Optimal design of ultrasonic transducer based on multi-layer backing with adjustable impedance," *Ceram. Int.*, vol. 50, no. 23, pp. 51693–51700, Dec. 2024, doi: 10.1016/j.ceramint.2024.02.006.

[13] J. Yen and Z. Nussbaum, "Active Damping of Air-backed Ultrasonic Transducers Using Arbitrary Waveform Generators," in *2020 IEEE International Ultrasonics Symposium (IUS)*, Las Vegas, NV, USA: IEEE, Sep. 2020, pp. 1–4. doi: 10.1109/IUS46767.2020.9251816.

[14] P. Allisy-Roberts and J. Williams, "Imaging with ultrasound," in *Farr's Physics for Medical Imaging*, Elsevier, 2008, pp. 147–168. doi: 10.1016/B978-0-7020-2844-1.50013-2.

[15] C. Fei *et al.*, "Design of matching layers for high-frequency ultrasonic transducers," *Appl. Phys. Lett.*, vol. 107, no. 12, p. 123505, Sep. 2015, doi: 10.1063/1.4931703.

[16] J. S. Jeong, J. M. Cannata, and K. K. Shung, “Adaptive HIFU noise cancellation for simultaneous therapy and imaging using an integrated HIFU/imaging transducer,” *Phys. Med. Biol.*, vol. 55, no. 7, pp. 1889–1902, Apr. 2010, doi: 10.1088/0031-9155/55/7/007.

[17] V. T. Rathod, “A Review of Acoustic Impedance Matching Techniques for Piezoelectric Sensors and Transducers,” *Sensors*, vol. 20, no. 14, p. 4051, Jul. 2020, doi: 10.3390/s20144051.

[18] T. Zhang, Y. Zhou, and Z. Wang, “In Situ Measurement of Acoustic Attenuation for Focused Ultrasound Ablation Surgery Using a Boiling Bubble at the Focus,” *Ultrasound Med. Biol.*, vol. 49, no. 7, pp. 1672–1678, Jul. 2023, doi: 10.1016/j.ultrasmedbio.2023.02.014.

[19] “IEC 60601-1:2024 SER.” Accessed: Apr. 10, 2025. [Online]. Available: https://webstore.iec.ch/en/publication/2603

[20] F. A. Duck, H. C. Starritt, G. R. Ter Haar, and M. J. Lunt, “Surface heating of diagnostic ultrasound transducers,” *Br. J. Radiol.*, vol. 62, no. 743, pp. 1005–1013, Nov. 1989, doi: 10.1259/0007-1285-62-743-1005.

[21] A. A. E. D. Bishay *et al.*, “Preliminary Examination of the Effects of Focused Ultrasound on Living Skin and Temperature at the Skin-Transducer Interface,” *Bioeng. Basel Switz.*, vol. 11, no. 11, p. 1126, Nov. 2024, doi: 10.3390/bioengineering11111126.

[22] *IEC 60601-2-37 IEC 60601-2-37:2024 Medical electrical equipment - Part 2-37: Particular requirements for the basic safety and essential performance of ultrasonic medical diagnostic and monitoring equipment*, 2024.

[23] M. Muhr, V. Nikolić, B. Wohlmuth, L. Wunderlich, ,Technical University of Munich, Department of Mathematics, Chair of Numerical Mathematics, Boltzmannstraße 3, 85748 Garching, Germany, and ,Queen Mary University of London, School of Mathematical

Sciences, Mile End Road, London E1 4NS, United Kingdom, “Isogeometric shape optimization for nonlinear ultrasound focusing,” *Evol. Equ. Control Theory*, vol. 8, no. 1, pp. 163–202, 2019, doi: 10.3934/eect.2019010.

[24] *ISO 10993-1:2009 Biological evaluation of medical devices Part 1: Evaluation and testing within a risk management process*, 2009.

[25] M. M. El-Desouki and K. Hynynen, “Driving circuitry for focused ultrasound noninvasive surgery and drug delivery applications,” *Sensors*, vol. 11, no. 1, pp. 539–556, 2011, doi: 10.3390/s110100539.

[26] Y. N. Kumar *et al.*, “A comparative study of histotripsy parameters for the treatment of fibrotic ex-vivo human benign prostatic hyperplasia tissue,” *Sci. Rep.*, vol. 14, no. 1, p. 20365, Sep. 2024, doi: 10.1038/s41598-024-71163-2.

[27] W. Legon, L. Ai, P. Bansal, and J. K. Mueller, “Neuromodulation with single-element transcranial focused ultrasound in human thalamus,” *Hum. Brain Mapp.*, vol. 39, no. 5, pp. 1995–2006, May 2018, doi: 10.1002/hbm.23981.

[28] A. Javid, R. Biswas, S. J. Ilham, and M. Kiani, “High-Voltage Phased Array Electronics for Ultrasound Neuromodulation,” in *2024 IEEE 67th International Midwest Symposium on Circuits and Systems (MWSCAS)*, Springfield, MA, USA: IEEE, Aug. 2024, pp. 543–546. doi: 10.1109/MWSCAS60917.2024.10658940.

[29] M. G. Mallay, T. G. Landry, and J. A. Brown, “An 8 mm endoscopic histotripsy array with integrated high-resolution ultrasound imaging,” *Ultrasonics*, vol. 139, p. 107275, Apr. 2024, doi: 10.1016/j.ultras.2024.107275.

[30] Z. Izadifar, Z. Izadifar, D. Chapman, and P. Babyn, “An Introduction to High Intensity Focused Ultrasound: Systematic Review on Principles, Devices, and Clinical Applications,” *J. Clin. Med.*, vol. 9, no. 2, p. 460, Feb. 2020, doi: 10.3390/jcm9020460.

[31] P. M. Holmes, H.-K. Lee, and M. W. Urban, “F-number optimization for synthetic aperture delay-multiply-and-sum reconstruction,” *Ultrasonics*, vol. 136, p. 107158, Jan. 2024, doi: 10.1016/j.ultras.2023.107158.

[32] Y. Kim, A. D. Maxwell, T. L. Hall, Z. Xu, K.-W. Lin, and C. A. Cain, “Rapid prototyping fabrication of focused ultrasound transducers,” *IEEE Trans. Ultrason. Ferroelectr. Freq. Control*, vol. 61, no. 9, pp. 1559–1574, Sep. 2014, doi: 10.1109/TUFFC.2014.3070.

[33] H. Sheppard, “Development of HIstotripsy Focused Ultrasound Devices Using Rapid Prototyping Methods,” Virginia Tech, Blackburg VA, 2022.

[34] N. Dodoo, “Design and Development of Single Element Focused Ultrasound Transducers,” Virginia Tech, Blackburg VA, 2024.

[35] A. Kafle, E. Luis, R. Silwal, H. M. Pan, P. L. Shrestha, and A. K. Bastola, “3D/4D Printing of Polymers: Fused Deposition Modelling (FDM), Selective Laser Sintering (SLS), and Stereolithography (SLA),” *Polymers*, vol. 13, no. 18, p. 3101, Sep. 2021, doi: 10.3390/polym13183101.

[36] “Technical Considerations for Additive Manufactured Medical Devices - Guidance for Industry and Food and Drug Administration Staff”.

[37] K. B. Bader, E. Vlaisavljevich, and A. D. Maxwell, “For Whom the Bubble Grows: Physical Principles of Bubble Nucleation and Dynamics in Histotripsy Ultrasound Therapy,” *Ultrasound Med. Biol.*, vol. 45, no. 5, pp. 1056–1080, May 2019, doi: 10.1016/j.ultrasmedbio.2018.10.035.

[38] A. D. Maxwell *et al.*, “Cavitation clouds created by shock scattering from bubbles during histotripsy,” *J. Acoust. Soc. Am.*, vol. 130, no. 4, pp. 1888–1898, Oct. 2011, doi: 10.1121/1.3625239.

[39] A. D. Maxwell, K. J. Haworth, C. K. Holland, S. A. Hendley, W. Kreider, and K. B. Bader, “Design and Characterization of an Ultrasound Transducer for Combined Histotripsy-Thrombolytic Therapy,” *IEEE Trans. Ultrason. Ferroelectr. Freq. Control*, vol. 69, no. 1, pp. 156–165, Jan. 2022, doi: 10.1109/TUFFC.2021.3113635.

[40] A. A. Seyhan, “Lost in translation: the valley of death across preclinical and clinical divide – identification of problems and overcoming obstacles,” *Transl. Med. Commun.*, vol. 4, no. 1, p. 18, Dec. 2019, doi: 10.1186/s41231-019-0050-7.

[41] “What is an IDE? | Clinical Center.” Accessed: Mar. 23, 2025. [Online]. Available: https://www.cc.nih.gov/orcs/ide/what-is-an-ide

[42] C. for D. and R. Health, “IDE Application,” *FDA*, Oct. 2024, Accessed: May 08, 2025. [Online]. Available: https://www.fda.gov/medical-devices/investigational-device-exemption-ide/ide-application

[43] “21 CFR Part 812 -- Investigational Device Exemptions.” Accessed: Mar. 23, 2025. [Online]. Available: https://www.ecfr.gov/current/title-21/part-812

Chapter 2: Regulatory Guidelines and Considerations

2.1 Introduction to Regulatory Requirements for Medical Devices

The development of FUS devices, like all medical devices, must navigate a complex regulatory landscape to ensure safety and efficacy before reaching clinical trials. In the United States, the Center for Devices and Radiological Health (CDRH) of the FDA sets out guidelines, which outline recommended practices to help manufacturers meet regulatory expectations [1]. Alongside these, standards define specific technical criteria that devices must meet to demonstrate compliance with safety and effectiveness requirements [2]. In contrast, codes refer to legally enforceable regulations that apply to device design and manufacturing [3]. Together, these regulatory frameworks ensure that high-risk devices like histotripsy transducers are developed with the necessary controls to minimize risks and maximize patient safety.

Moving a FUS device toward clinical use involves addressing key challenges in design, testing, and regulatory alignment. The proposed framework emphasizes safety-by-design principles, the application of relevant technical standards, and proactive risk management strategies to mitigate potential hazards. By incorporating design controls and aligning development efforts with regulatory expectations from the outset, this approach may help streamline the path to clinical evaluation, including compliance with requirements outlined in IDE applications [4]. By carefully identifying and managing potential risks, developers can establish a strong foundation that supports clinical readiness and enables the continued evolution of the device for broader medical or translational impact.

2.2 Risk Management

The development of medical devices depends on a foundation of trust between engineers and the patients who rely on these devices for safe and effective treatment. Patients typically do not focus on the potential risks associated with medical devices because they are often seen as essential tools for diagnostic or treatment purposes. Instead, they place their confidence in medical professionals, who are responsible for using these devices, and in regulatory systems that approve the devices for market use. Given their already vulnerable position, it is crucial to protect them from risks that could further compromise their health. Therefore, developers and manufacturers of medical devices must implement robust safety measures and controls to ensure their well-being.

International standard ISO 14971 for the application of risk management to medical devices [5] was developed to provide a framework for medical device manufacturers to identify the potential hazards, evaluate the associated risks, implement risk control measures, and monitor their effectiveness throughout the device's lifecycle. The risk management process described in ISO 14971 consists of several steps, as illustrated in **Figure 0-1**. Each step plays a role in ensuring that risks are systematically identified, evaluated, and mitigated throughout the medical device lifecycle.

Figure 0-1. An overview of the key steps in risk management according to ISO 14971, including risk analysis, risk evaluation, risk control, evaluation of overall residual risk, risk management review, and production and post-production activities.

The first step in the risk management process is risk analysis, which involves documenting the intended use of the medical device, identifying potential hazards, and estimating the associated risks. A well-defined description of the intended use helps establish the limits of the proper application of the medical device, while any usage outside of these boundaries is considered misused. Understanding how the device is intended to function, it becomes easier to identify potential hazards which are sources of harm that could stem from the device, its use, or its environment. These can include energy hazards, biological and chemical hazards, as well as operational and information hazards. After identifying the potential hazards, the risks associated with each hazard are estimated by evaluating the severity of harm and the probability of occurrence. Probability of occurrence refers to the likelihood of a hazard happening, while severity describes the extent of harm that could result from the hazardous situation. Estimating these factors can be challenging, particularly for new products or when limited data is available. As a result, these estimates often rely on expert judgment and the best available information. **Table 1** and

Table 2 provides the severity and occurrence levels, along with their corresponding descriptions, to guide this process. To systematically evaluate and prioritize risks based on their probability of occurrence and severity, manufacturers often use a risk matrix shown in

Table 3. This tool visually represents risks by plotting probability on one axis and severity on the other, creating a grid that categorizes risks into levels such as low, medium, and high. By providing a clear and structured way to assess risks, the risk matrix helps manufacturers make informed decisions about which risks require immediate attention and which can be considered acceptable. However, all hazardous situations and types of harm need to be considered because less severe situations, but frequent occurrence can still result in high risk.

Table 1: Severity Levels for Risk Analysis

Level	Category	Description
1	Negligible	No injury or adverse health effect to patient or user
2	Minor	Temporary discomfort or minor injury; no medical intervention
3	Serious	Temporary injury or impairment requiring medical intervention
4	Major	Major injury, permanent impairment, or life-threatening condition
5	Catastrophic	Patient or user death or severe permanent disability

Table 2: Occurrence Levels for Risk Analysis

Level	Category	Description
1	Improbable	Highly unlikely to occur during device lifetime
2	Remote	Not expected to occur during device lifetime
3	Occasional	May occur once during device lifetime
4	Probable	Likely to occur multiple times during device lifetime
5	Frequent	Expected to occur regularly during device lifetime

Table 3: Risk assessment matrix showing the relationship between severity and occurrence levels. This matrix provides a framework for evaluating and prioritizing risks based on the level, where high risk rating (red) is an unacceptable risk, medium risk (orange) is an important risk, and low risk (green) is an acceptable risk

Probability of Occurrence						
	Frequent (5)	Low	Medium	High	High	High
	Probable (4)	Low	Medium	High	High	High
	Occasional (3)	Low	Low	Medium	High	High
	Remote (2)	Low	Low	Medium	Medium	High
	Improbable (1)	Low	Low	Low	Medium	Medium
		Negligible (1)	Minor (2)	Serious (3)	Major (4)	Critical (5)
		Severity of Impact				

Once risks are identified and estimated, the next step is risk evaluation, where the manufacturer determines their acceptability, and then ranks and decides which risks need to be controlled. Typically, the low level corresponds to acceptable risks, the high level indicates unacceptable risks that must be addressed through mitigation measures, and the medium level represents risks that should be reduced as low as reasonably possible. For those that exceed acceptable limits, risk control measures are implemented to reduce or mitigate risks to an acceptable level. This is achieved through the following order of controls, including inherent safety by design, protective measures, and information for safety, such as labels and warnings. Afterward, the evaluation of overall residual risk is conducted to ensure that the remaining (residual) risk after controls are applied is acceptable. The effectiveness of the risk management process and controls are then reviewed. Documentation is prepared to report findings, including how risks were controlled, the residual risk level, and any unresolved issues to transparency and accountability. During the production phase, the risk management plan is actively applied. Risks are continuously monitored, and controls are enforced to ensure safety and quality throughout the manufacturing or operational process. The final step is post-production, which involves the ongoing monitoring of

the device through real-world use, customer feedback, and post-market surveillance. Data collected during this phase is carefully analyzed to identify any new risks or unforeseen issues that may emerge throughout the product's lifecycle. Insights gained from this analysis are then fed back into the risk management process, enabling continuous improvement and ensuring that the product remains safe and effective over time.

Table 4 serves as an example of how the outlined risk management approach can be applied. It focuses on a histotripsy transducer designed for endoscopic (transesophageal) use, intended for tissue destruction in the pancreas, liver, or other organs. The transducer is mounted at the distal tip of a flexible endoscope and manually positioned by a physician to the target site. Ultrasound imaging is integrated to guide placement and monitor treatment, providing real-time feedback during the procedure. The table illustrates how potential hazards were identified, assessed, and addressed during early-stage design. Using the principles of ISO 14971, each risk was evaluated based on its likelihood and severity, then paired with specific design strategies intended to reduce or eliminate the risk. For example, thermal risk at the transducer surface was initially rated as high but can be reduced through the inclusion of passive cooling features. Mechanical risks, such as perforation or component detachment during insertion, can be mitigated with rounded edges, mechanical stress testing, and a protective sheath. However, some risks remain high despite design efforts. The biological (material) risk is still rated high because biocompatibility must be confirmed through standardized testing, not assumed based on manufacturer data. Electrical shock remains a concern due to the use of high voltage near tissue and fluid; mitigation requires formal electrical safety testing. Similarly, acoustic risks like off-target energy delivery cannot be fully addressed through design alone and must be evaluated through beam measurements and characterization. These three risks, which include

biocompatibility, electrical safety, and acoustic output, represent the highest priority hazards identified through the risk analysis and will serve as the primary focus of this thesis. Together, they illustrate how certain hazards require verification testing to supplement design controls as part of a complete risk management approach. **Appendix A.** Example of Risk Assessment For FUS Devices contains a more comprehensive risk analysis covering a wider range of potential hazards relevant to focused ultrasound device development.

Table 4. Risk assessment for a rapid-prototyped histotripsy transducer intended for endoscopic use. Risks were identified across thermal, electrical, mechanical, biological, chemical, acoustic, and user-related domains. Each risk was rated before and after proposed design mitigations based on a structured risk analysis framework following ISO 14971.

Risk Type	Description	Risk Rating	Mitigation through design	New Risk Rating
Diagnostic	Limited imaging due to GI tract interference during targeting	**High**	Imaging probe	Low
Thermal	Overheating at the transducer's surface during treatment	**High**	Built-in cooling	Low
Mechanical	Transducer or component detaches within GI tract	Low	Mechanical stress testing	Low
Mechanical	Perforation during insertion of the device	**High**	Round edges + sheath	Low
Mechanical/Electrical	Device is cracked but is still used	**High**	Material selection	Low
Chemical	The material degrades due to exposure of high/low pH	Low	Sheath	Low
Biological (Infection)	Inadequate sterilization or disinfection prior to insertion	**High**	Sheath	Low
Biological (Material)	Transducer housing cause reaction in tissue	**High**	Sheath + biocompatibility test	**High**
Electrical Shock	Leakage or unintended contact with high-voltage	**High**	Electrical safety test	**High**
Acoustic	Off-target acoustic injury to nearby tissue	**High**	Acoustic characterization	**High**
Acoustic/Electrical	Incorrect treatment parameters set by the user	Medium	Single pre-set treatment	Low
User Error	Operator misidentifies the target treatment zone	Low	Operator training and credentialing	Low

2.3 Design Controls

Design controls, as defined by the FDA's Quality System Regulation (21 CFR 820.30) [6], provide a structured framework for designing medical devices to meet user needs and regulatory requirements. They work together with risk management to ensure devices are safe and effective. While risk management focuses on identifying and addressing potential hazards, design controls integrate these risk mitigation strategies into the development process. To visualize how this

integration works **Figure 0-2.** demonstrates the stages of the design control process and how they align with risk management principles.

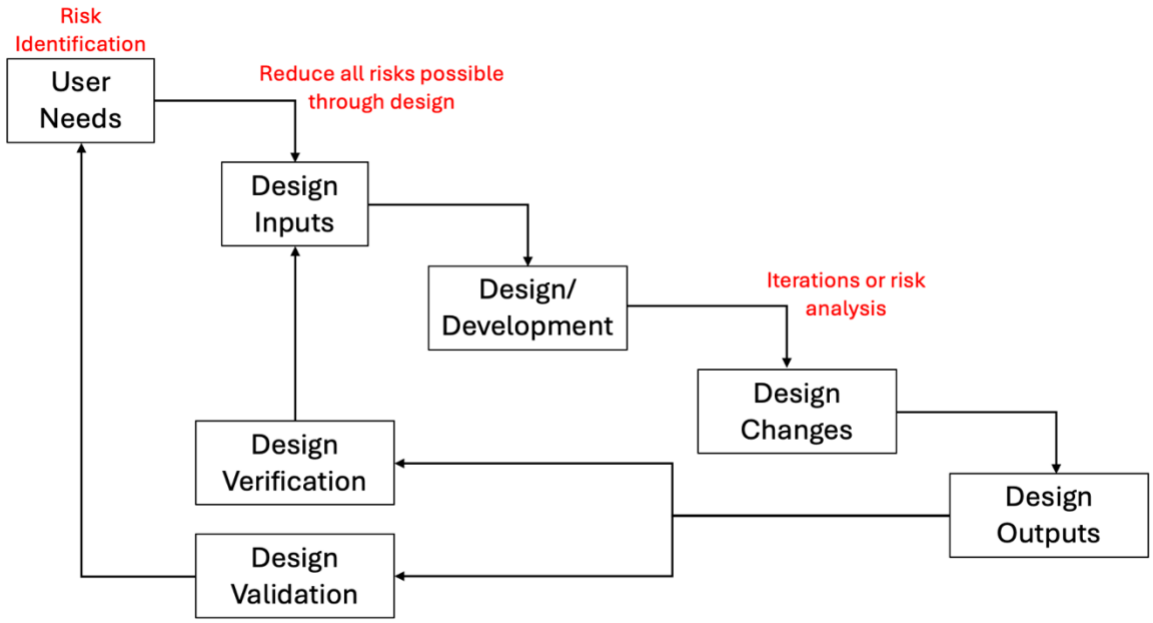

Figure 0-2. This figure illustrates the systematic flow of design controls with risk management integration throughout the medical device development process. The flow chart demonstrates how risk management activities inform and interact with each phase of design controls, ensuring that potential hazards are identified early and mitigated effectively before product release.

The process begins with understanding and defining the user needs. User needs refer to understanding the general purpose and specific requirements of the end users (i.e. patients and clinicians), which are captured through intended use and indications for use. Intended use defines the overall function or purpose of the device, while indications for use describes the specific conditions or diseases the device will address and the target patent population. For example, in histotripsy, a user need might be treating pancreatic tumors without harming nearby healthy tissue. Alongside user needs, risk management begins by identifying and assessing potential hazards, such as unintended cavitation causing damage to nearby organs, adverse tissue reaction, or electrical shock. Next, the team turns user needs into specific, measurable requirements, called design inputs. These inputs are then transformed into design outputs, such as prototypes, Computer-aided Design

(CAD) models, and specifications, which must align with the inputs and meet regulatory requirements. For FUS, this might include acoustic characterization like acoustic output power, frequency, and focal depth. Additionally, risk mitigation strategies are implemented through design such as fail-safe mechanisms or using biocompatible materials. During the design and development process, engineers translate these inputs into physical prototypes by selecting appropriate materials, designing transducer geometry, and incorporating features that optimize performance. As development progresses, design changes may be necessary based on test results, risk assessments, or new clinical insights. These changes are reassessed to ensure they do not introduce new risks. Then the finalized design leads to design outputs which are the final documents, drawings, and specifications that show how device will be made, tested, and used to meet design requirements. Once the device design is completed, the team performs design verification to confirm that the outputs meet the inputs through testing, analysis, or inspections (i.e. If the device is designed as expected). For FUS, this might involve testing measuring the acoustic field to ensure consistency with simulations and requirements. After that, design validation tests the device in real-world conditions and meets the original user needs like treating patients with pancreatic tumors to prove it is safe and effective. Integrating risk management into design controls allows potential issues to be addressed early in the design and prototype phases, ensuring that safety is built into the device from the very beginning.

2.4 International and Industry Standards

The structured use of risk management and design controls helps ensure that medical devices are safe, effective, and appropriate for their intended use. ISO 14971 provides the foundation for this process by outlining how to identify, evaluate, and control risks throughout the device lifecycle. In addition to ISO 14971, other international standards support risk-based

approaches for specific aspects of device safety. ISO 10993 provides a framework for evaluating the biocompatibility of materials in contact with the body [7], while IEC 60601-1 defines general safety and essential performance requirements for electrical medical equipment [8]. This thesis focuses on a subset of these standards that directly address the highest-priority risks identified in the risk management process, including biocompatibility, electrical safety, and acoustic output. These standards were selected not only for their technical relevance to focused ultrasound systems, but also because they are formally recognized by the FDA as part of regulatory submissions. For example, the FDA's guidance document on the use of ISO 10993 outlines how to apply biocompatibility testing standards during preclinical evaluation of medical devices. Similarly, the FDA's guidance on diagnostic ultrasound systems and transducers references IEC 60601-1 and related documents, including IEC 60601-2-37 and IEC 62127-1, for measuring acoustic output and assessing thermal and mechanical effects [9]. By grounding the testing approach in both international standards and FDA-recognized guidance documents, this work aims to support the development of focused ultrasound systems that are aligned with clinical and regulatory expectations.

2.4.1 ISO 10993: Biocompatibility of Medical Devices

ISO 10993 is a series of international standards that covers various aspects of biocompatibility of materials used in medical devices, ensuring they are safe for human contact. It evaluates the potential for adverse biological reactions, such as toxicity, irritation, or sensitization, which could occur when a device interacts with the body. The FDA incorporates ISO 10993 into its regulatory framework by using it as a recognized consensus standard for medical device approval. Manufacturers submitting devices for FDA clearance or approval must demonstrate compliance with ISO 10993 through appropriate testing and risk assessments. ISO 10993-1 [7] is

a crucial part of the ISO 10993 series, providing guidelines for the biological evaluation of medical devices. This standard is based on a risk evaluation framework that helps manufacturers determine the appropriate biocompatibility tests required for a device. It considers various factors, such as the materials used in the device, the duration of contact with the body [3], and the type of contact (e.g., direct or indirect) [7]. By conducting a thorough risk assessment, ISO 10993-1 ensures that testing is tailored to the specific device and its intended use, minimizing unnecessary testing while addressing potential safety concerns. Therefore, this standard is particularly important for FUS devices as they can come into direct or indirect contact with patients. Direct contact refers to parts of a medical device that physically touch or interact with the body, while indirect contact involves components that allows a fluid or gas to pass through it before reaching body, but the device itself does not touch the body directly. The standard outlines a series of tests based on the contact type and duration of contact shown in

Table 5. Devices are categorized by their contact type through the skin, intact mucosal membrane, breached or compromised skin, or internal tissues. Duration refers to how long the device or its components are in contact with the body every day for any portion of a day. It is categorized based on the total exposure period on a single patient, which is further divided into limited exposure (< 24 hours), prolonged exposure (>24 hours but not > 30 days), and long-term exposure (> 30 days). To calculate the total exposure period, one must assess the length of time the device is actively in use or in contact with the body between the first and last use of the medical device. One example outlined in ISO 10993, in a scenario where a device comes into contact with tissues daily, such as a single-use disposable feeding tube that is replaced several times during a patient's treatment with a feeding pump system (e.g., 2 hour of use every day for 14 days), it would be categorized as having a prolonged contact duration [3]. Another example given in ISO 10993

is a device with intermittent contact with tissues, such as administration sets for infusion pumps. These devices are used only a few times a year, like a 1-hour treatment every 6 months over a span of 3 years [7]. Intermittent contact refers to devices that are used occasionally where there is a period of greater than 24 hours between contact use. If justified, this usage would total 6 contact days, and the device would be categorized as having prolonged exposure [7]. By understanding the type and duration of contact, one can refer to

Table 5 to identify and evaluate the necessary biological tests to ensure the device is safe for its intended use.

Table 5: Adapted from ISO 10993-1:2009 [10] showing potential biological evaluation tests based on the nature of body contact and duration of exposure. Categories include surface, external communicating, and implant devices, with exposure durations classified as limited (<24 h), prolonged (24 h–30 days), and permanent (>30 days). Crosses indicate biological endpoints that may require evaluation depending on risk analysis. Additional testing is not needed if existing data sufficiently address the biological safety endpoints.

Medical device categorization by			Biological effect							
nature of body contact (see 5.2)		contact duration (see 5.3) A – limited (⩽ 24 h) B – prolonged (> 24 h to 30 d) C – permanent (> 30 d)	Cytotoxicity	Sensitization	Irritation or intracutaneous reactivity	Systemic toxicity (acute)	Subchronic toxicity (subacute toxicity)	Genotoxicity	Implantation	Haemocompatibility
Category	Contact									
Surface device	Skin	A	X [a]	X	X					
		B	X	X	X					
		C	X	X	X					
	Mucosal membrane	A	X	X	X					
		B	X	X	X					
		C	X	X	X		X	X		
	Breached or compromised surface	A	X	X	X					
		B	X	X	X					
		C	X	X	X		X	X		
External communicating device	Blood path, indirect	A	X	X	X	X				X
		B	X	X	X	X				X
		C	X	X		X	X	X		X
	Tissue/bone/dentin	A	X	X	X					
		B	X	X	X	X	X	X	X	
		C	X	X	X	X	X	X	X	
	Circulating blood	A	X	X	X	X				X
		B	X	X	X	X	X	X	X	X
		C	X	X	X	X	X	X	X	X
Implant device	Tissue/bone	A	X	X	X					
		B	X	X	X	X	X	X	X	
		C	X	X	X	X	X	X	X	
	Blood	A	X	X	X	X	X		X	X
		B	X	X	X	X	X	X	X	X
		C	X	X	X	X	X	X	X	X

While the type and duration of contact help determine the required biological testing, ISO 10993-1 and the FDA guidance document highlight that chemical characterization of the materials used in the device can also play a key role in justifying or potentially reducing the need for certain tests. Chemical characterization involves identifying and quantifying the chemical constituents of a device's materials, including additives, processing aids, and potential leachable or extractables that could interact with the patient. Once the chemical constituents are identified, a toxicological risk assessment is conducted to evaluate their potential to cause harm and determine whether additional testing is necessary. For instance, if a material contains known genotoxic or

carcinogenic constituents, additional testing would be required to ensure the device does not pose a risk of DNA damage or cancer. Likewise, systemic toxicity (e.g. acute, sub-acute, sub-chronic, and chronic) can be assessed through a toxicological risk evaluation because it relies on the quantitative analysis of chemical constituents and their potential to cause harm at various exposure levels, which can be compared to established safety thresholds [7]. In contrast, cytotoxicity, irritation, and sensitization are localized biological responses that depend on direct tissue interaction and cannot be fully predicted through chemical characterization alone. These tests are necessary for all medical devices regardless of the type and contact duration. As discussed in chapter 1, most histotripsy prototypes are fabricated using 3D-printed materials. However, 3D-printed medical devices are not yet widely adopted in clinical settings due to several challenges, including material limitations, speed and scalability, cost, lack of standardization, and durability [11]. Consequently, these materials are not well-characterized in terms of biocompatibility, and there is limited data available on their chemical composition. To bridge the gap from FUS prototypes to clinical trials, this thesis aims to establish a foundational framework for biological evaluation. This framework will ensure that materials in contact with patients are safe, biocompatible, and free from potential harm, thereby facilitating their transition into clinical translation.

2.4.2 IEC 60601-1: Basic Safety and Essential Performance of Medical Electrical Equipment

The IEC 60601-1 is an international standard, published by the International Electrotechnical Commission (IEC), that outlines safety and performance requirements for medical electrical equipment [8]. It is widely adopted across the globe and serves as a reference for manufacturers, regulators, and healthcare providers. The standard aims to ensure that electrical

medical devices operate reliably while minimizing risks to patients, operators, and the environment. Its requirements cover a broad range of considerations, including electrical safety, mechanical integrity, thermal management, and electromagnetic compatibility, as well as a systematic risk management process to identify and address potential hazards. Compliance with IEC 60601-1 is often a prerequisite for regulatory approval, making it an essential framework for the development and commercialization of medical devices.

FUS devices are subject to compliance with IEC 60601-1 due to the inherent risks they pose in clinical environments. These devices often involve high-voltage power supplies, complex electronics, and patient interaction, making them susceptible to electrical shock hazards. The risk of electrical shock is a primary concern because it can lead to serious injury or even death. Electrical shock occurs when a person becomes part of the electrical circuit, allowing current to flow through their body. This current can disrupt normal physiological functions and cause a range of harmful effects, depending on the amount of current and the duration of exposure. When a person experiences an electrical shock, the impact largely depends on the current flowing through the body, which is influenced by the voltage of the electrical source and the resistance of the body. Even relatively low currents, in the range of 9-30 mA, can cause painful shocks, muscle contractions, and difficulty in releasing the source of the shock [12]. If the current exceeds 30 mA, it can lead to more severe consequences, such as respiratory paralysis, where the victim may be unable to breathe, and ventricular fibrillation, a life-threatening heart arrhythmia [12]. At higher currents (100 mA or more), the risk of death increases significantly due to the potential for fatal arrhythmias and cardiac arrest [12]. To address these risks, IEC 60601-1 mandates a series of tests with the goal minimize risks such as electrical shock, insulation failure, improper grounding, and unintended current flow.

Most tests under IEC 60601-1 depend on how medical electrical equipment is classified based on factors such as intended use, patient contact, and power source. Devices are categorized into Class I or Class II based on their method of protection against electric shock [8]. Class I devices rely on a protective earth connection as a primary safety measure, ensuring that any fault current is safely diverted to the ground. These devices typically have a three-prong plug and require ground bond testing to verify the integrity of the earth connection. In contrast, Class II devices do not rely on a protective earth and instead use double or reinforced insulation to prevent electric shock. These devices often have a two-prong plug and are designed to be safer in environments where grounding may be unreliable. In addition to these classifications, medical devices are further categorized based on the type of applied parts which are components that come into direct or indirect contact with the patient. These categories include Type B (Body), Type BF (Body Floating), and Type CF (Cardiac Floating). Type B applied parts are typically used for non-invasive applications and have the least stringent leakage current requirements. Type BF applied parts are isolated from the ground and are used for applications where the device may come into contact with the patient's body but not the heart. Type CF applied parts are the most stringent category and are designed for direct cardiac contact, such as in devices used for electrophysiology or cardiac monitoring. FUS devices, depending on their application, may fall into any of these categories, but they often require Type BF or CF classification due to their potential for direct or indirect patient contact.

The classification of a device (Class I or II) and the type of applied part (B, BF, or CF) directly influence the testing requirements under IEC 60601-1 [8]. For example, Class I devices must undergo ground bond testing to ensure the protective earth connection is reliable, while Class II devices are exempt from this test but must meet stricter insulation requirements.

Similarly, devices with Type BF or CF applied parts must meet more stringent leakage current limits compared to those with Type B applied parts. These distinctions ensure that the level of safety testing aligns with the potential risks associated with the device's intended use.

Furthermore, a key concept in IEC 60601-1 is the evaluation of devices under single fault conditions [8]. This means testing the device to ensure it remains safe even if one safety mechanism fails. For example, if the protective earth connection in a Class I device were to break, or if the insulation in a Class II device were to degrade, the device must still prevent electric shock or other hazards. Single fault conditions are simulated during testing to evaluate the device's ability to maintain safety in worst-case scenarios. This is particularly important for medical devices, as they must operate reliably even in the event of a failure. For FUS devices, which often involve high voltages and patient contact, testing under single fault conditions ensures that the device remains safe even if a component malfunction. To conduct these tests, manufacturers use an electrical safety analyzer, a specialized tool designed to measure leakage currents and other electrical parameters in medical devices. This analyzer simulates normal and fault conditions to ensure the device's electrical safety and compliance with IEC 60601-1.

One of the tests mandated by the standard is ground bond testing, which verifies the integrity of the protective earth connection in Class I devices [8]. This ensures that the ground path can safely carry fault currents without excessive resistance, reducing the risk of electric shock. For FUS devices, which are typically connected to an amplifier box powered by a three-prong cord and high-voltage power supplies, a reliable ground connection is crucial for ensuring safety. Another important test is dielectric strength testing or also referred to as high potential (Hipot) testing, which evaluates the insulation's ability to withstand high voltages without breaking down. During this test, a high voltage is applied between live parts and the chassis or ground, and the

insulation is monitored for failure. This is particularly important for FUS devices, as their high-voltage components must remain electrically isolated from patients and operators to prevent shock hazards. IEC 60601-1 also requires several leakage current tests to measure unintended current flow that could pose risks to patients or operators. Earth leakage current testing measures the current escaping to the protective earth, ensuring it stays within safe limits [8]. Enclosure leakage current testing checks for unintended current on the device's outer casing, which is important for preventing risks to anyone touching the device [8]. Patient leakage current testing measures unintended current that could flow through a person to earth from the applied part [8]. Finally, patient auxiliary current testing ensures that minimal current flows between parts connected to the patient[8]. All the different types of tests can be summarized in **Table 6.**

Table 6: Summary of electrical safety tests for FUS devices, indicating the specific risks mitigated by each test and their relevance to device development and safety.

Test Type	Risk Mitigated	Relevance to FUS Devices
Ground Bond	Prevents electric shock from inadequate grounding	Ensures proper grounding of Class I FUS power supply
Dielectric Strength (Hipot)	Prevents electrical breakdown of insulation reducing shock risks	Verifies the insulation's ability to withstand high voltage in FUS components
Earth Leakage	Minimizes risk of shock from leakage to ground	Checks for unintentional current flow to ground in FUS devices
Enclosure Leakage	Prevent electric shock from the device's outer surface	Verifies that the external casing of FUS devices remains safe to touch
Patient Leakage	Prevents risk of shock to the patient through applied parts	Ensures no harmful electrical current flows through patient contacting parts during use of FUS devices
Patient Auxiliary Leakage	Prevents cross-leakage current between applied parts and patient	Verifies minimal current flow between connected parts and the patient

Together, these tests form a comprehensive evaluation of the electrical safety of FUS devices, ensuring they meet the stringent requirements of IEC 60601-1. By addressing risks such as electric shock, insulation failure, and unintended current flow, these tests play a role in ensuring that FUS systems can be safely integrated into clinical practice. Compliance with these testing requirements is not only necessary for regulatory approval but also helps build trust among healthcare providers and patients, who rely on these technologies for safe and effective treatment. Through this rigorous testing framework, IEC 60601-1 helps ensure that FUS devices deliver the highest levels of safety and performance, ultimately benefiting patients and advancing the field of therapeutic ultrasound.

2.4.3 IEC: Acoustic characterization

The FDA's guidance document for marketing clearance of diagnostic ultrasound systems and transducers defines exposure limits for key acoustic parameters, including spatial-peak temporal-average intensity (I_{SPTA}) and spatial-peak pulse-average intensity (I_{SPPA}) [9]. The guidance recommends that I_{SPTA} remain below 720 mW/cm² to limit thermal exposure, and that I_{SPPA} not exceed 190 W/cm² to reduce mechanical effects [9]. Although these thresholds were developed for diagnostic imaging, they provide a reference framework for evaluating early-stage therapeutic devices, especially for safety documentation and reporting. In this thesis, I_{SPTA} and I_{SPPA} are calculated to assess whether the acoustic output of the histotripsy system aligns with or exceeds these reference values. Acoustic characterization aims to address two main questions: whether the system produces the intended therapeutic effect, and whether energy is delivered to the appropriate location. To evaluate therapeutic effect, this work reports I_{SPPA}, I_{SPTA}, and peak negative pressure (p-). I_{SPPA} quantifies the energy delivered per pulse at the point of highest intensity, and I_{SPTA} incorporates pulse repetition to provide a time-averaged exposure metric.

Although there is no regulatory threshold for peak negative pressure in histotripsy, cavitation is the primary mechanism of action, and it only occurs when p- exceeds a medium-dependent threshold. Therefore, measuring p- helps determine whether the pulses are sufficient to achieve the desired cavitation-based effect and where cavitation may occur. Spatial targeting is assessed through beam dimensions, focal length, and focal alignment with imaging. Beam dimensions are measured using the full width at half-maximum (FWHM) of the lateral and axial pressure profiles, which defines the spatial extent where the pressure remains above half of its peak negative value [13]. This measurement is used to assess how tightly focused the energy is, particularly if the beam extends beyond the boundaries of the intended treatment region. Focal length indicates the distance from the transducer to the point of peak intensity and is used to verify targeting depth. Focal alignment compares the actual location of the acoustic focus with the target identified by the image guidance system to ensure that the system delivers energy where intended. These acoustic measurements follow hydrophone-based methods described in IEC 62127-1, which provides standardized protocols for evaluating ultrasound fields in three dimensions under controlled conditions [13]. While IEC 60601-2-62 primarily addresses thermal-based high-intensity therapeutic ultrasound (HITU) devices, its safety principles regarding output verification, beam targeting, and exposure control can be adapted to non-thermal systems such as histotripsy [14]. By combining FDA-referenced thresholds with international standards and a risk-based selection of parameters, this thesis provides a consistent and reproducible methodology for characterizing the acoustic performance of early-stage focused ultrasound systems. All the different types of parameters can be summarized in **Table 7**.

Table 7. Summary of acoustic characterization tests for FUS devices, indicating the specific risks mitigated by each test and their relevance to device development and safety.

Measurement Type	Risk Mitigated	Relevance to FUS Devices
I_{SPPA}	Limits mechanical bioeffects from individual pulses	Measures pulse-level acoustic intensity; useful for evaluating mechanical exposure
I_{SPTA}	Limits cumulative thermal exposure	Captures time-averaged intensity over pulse cycles; compared against FDA limits
Peak Negative Pressure (p^-)	Ensures cavitation occurs only within controlled thresholds	Primary determinant for cavitation; used to confirm therapeutic effect is likely and localized
Beam Dimensions (FWHM)	Reduces risk of off-target energy delivery	Quantifies lateral and axial beam spread to ensure spatial confinement of acoustic focus
Focal Length	Confirms energy reaches intended anatomical depth	Verifies that acoustic energy is focused at the desired treatment distance
Focal Alignment	Prevents misalignment between image guidance and energy delivery	Ensures what appears on the image corresponds to the true acoustic focal point

References

[1] C. for D. and R. Health, "Guidance Documents (Medical Devices and Radiation-Emitting Products)," FDA. Accessed: May 08, 2025. [Online]. Available: https://www.fda.gov/medical-devices/device-advice-comprehensive-regulatory-assistance/guidance-documents-medical-devices-and-radiation-emitting-products

[2] "Recognized Consensus Standards: Medical Devices." Accessed: May 08, 2025. [Online]. Available: https://www.accessdata.fda.gov/scripts/cdrh/cfdocs/cfstandards/search.cfm

[3] C. for D. and R. Health, "Code of Federal Regulations (CFR)," *FDA*, Aug. 2023, Accessed: May 08, 2025. [Online]. Available: https://www.fda.gov/medical-devices/overview-device-regulation/code-federal-regulations-cfr

[4] C. for D. and R. Health, "IDE Application," *FDA*, Oct. 2024, Accessed: May 08, 2025. [Online]. Available: https://www.fda.gov/medical-devices/investigational-device-exemption-ide/ide-application

[5] *ISO 14971:2019 Medical devices — Application of risk management to medical devices*.

[6] "Design Control Guidance," *FDA*, 1997, [Online]. Available: https://www.fda.gov/media/116573/download

[7] *ISO 10993-1:2018 Biological evaluation of medical devices Part 1: Evaluation and testing within a risk management process*, 2018.

[8] *IEC 60601-1 – Medical electrical equipment – Part 1: General requirements for basic safety and essential performance*, 2024.

[9] "Marketing Clearance of Diagnostic Ultrasound Systems and Transducers - Guidance for Industry and Food and Drug Administration Staff".

[10] *ISO 10993-1:2009 Biological evaluation of medical devices Part 1: Evaluation and testing within a risk management process*, 2009.

[11] Y. Kim, A. D. Maxwell, T. L. Hall, Z. Xu, K.-W. Lin, and C. A. Cain, "Rapid prototyping fabrication of focused ultrasound transducers," *IEEE Trans. Ultrason. Ferroelectr. Freq. Control*, vol. 61, no. 9, pp. 1559–1574, Sep. 2014, doi: 10.1109/TUFFC.2014.3070.

[12] "Basic Electricity Safety," OSHA. [Online]. Available: https://www.osha.gov/sites/default/files/2019-04/Basic_Electricity_Materials.pdf

[13] *IEC 62127-1 IEC 62127-1:2022 Ultrasonics - Hydrophones - Part 1: Measurement and characterization of medical ultrasonic fields*, 2022.

[14] *IEC 60601-2-62 IEC 60601-2-62:2013 Medical electrical equipment - Part 2-62: Particular requirements for the basic safety and essential performance of high intensity therapeutic ultrasound (HITU) equipment*, 2013.

Chapter 3: Safety and Effectiveness Evaluation on Rapid Prototyped Histotripsy Single Element Transducer for Endoscopic Use

3.1 Introduction

Before advancing to complex multi-element histotripsy arrays, development begins with a single element transducer designed for endoscopic use. This simplified prototype enables early evaluation of baseline performance and validation of fundamental design principles. It also allows for early identification of technical or safety concerns while minimizing cost and complexity. Acoustic testing of a single element provides an initial indication of whether the design can achieve cavitation when scaled and integrated into more advanced systems. The selection of tests for this prototype, including materials evaluation, biocompatibility, electrical safety, and acoustic characterization, was guided by the risk analysis framework presented in Chapter 2, developed in accordance with ISO 14971 [1]. As discussed in Chapter 1, most 3D printed materials used in device housings and lenses are not fully characterized for acoustic applications [2]. Therefore, material testing in this chapter focuses on measuring sound speed, acoustic impedance, and attenuation to assess whether the selected materials support the transmission of focused ultrasound energy. These tests are carried out with consideration for risks associated with endoscopic use, including patient contact, electrical insulation, and targeting accuracy. **Table 8** summarizes how each test corresponds to the high priority risks identified earlier and outlines the mitigation strategies applied.

Table 8: Health risks and corresponding mitigation measures for FUS devices

Risks to Health	Mitigation Measures
Adverse tissue reaction	Biocompatibility evaluation (ISO 10993)
Electric shock	Electrical safety testing (IEC 60601-1)
Collateral tissue injury from ultrasound	Acoustic Characterization (IEC 60601-2-62/IEC 62127-1)

Risk management identifies testing priorities for FUS devices, while design controls ensure these requirements are addressed through a structured, traceable development process. This approach ensures each identified risk is met with an appropriate mitigation strategy, verified through regulatory-aligned testing. To keep engineering decisions aligned with what the users need, a design traceability matrix (**Table 9**) connects user requirements like "non-toxic materials" to design inputs such as cell viability ≤ 70%, and to verification methods like cytotoxicity testing per ISO 10995 [3]. This matrix maps each user need to its corresponding design input, design output, and verification method, in alignment with design control requirements outlined in chapter 2. Design validation typically involves demonstrating that the final device meets user needs under actual or simulated clinical conditions, therefore design validation is not addressed within this matrix, as it falls outside the scope of this thesis. **Table 9** below summarizes how user needs are translated into specific design requirements and verified through appropriate testing according to FDA guidelines and international recognized standards.

Table 9: Design Controls Traceability Matrix- Translation of User Needs into Design Requirements, Outputs, and Verification Methods in Accordance with International Standards (ISO 10993, IEC 60601-1, IEC 60601-2-62, and IEC 62127-1).

User Needs	**Design Input**	**Design Output**	**Design Verification**
Biocompatible and safe for contact.	Materials must meet ISO 10993-5 (Cell viability ≤ 70% indicates potential cytotoxic effects .	Transducer housing and patient-contacting components made from biocompatible materials.	Biocompatibility testing per ISO 10993.
Operate safely without risk of electrical shock.	Must meet IEC 60601-1 requirements: Leakage current < X µA for NC and < X µA for SFC. Passes ground bond test.	Device leakage current is designed to be ≤ X µA. Proper wiring to ensure device is grounded safely.	Electrical safety testing per IEC 60601-1.

Deliver acoustic energy precisely and accurately.	Device must produce acoustic parameters within safe thresholds (e.g., $I_{SPTA} < 720$ mW/cm²), with focused beam dimensions is less than the targeted tissue volume.	Transducer is designed to generate focused ultrasound with measurable I_{SPTA}, I_{SPPA}, and p- pressure values. Beam dimensions are engineered to achieve specific precision / volume requirements for targeted ablation	Acoustic testing per IEC 60601-2-62, IEC 62127-1, and FDA ultrasound guidance for parameter limits

3.2 Methods

3.2.1 Material Properties Testing

Four resins from *Formlabs* (Somerville, MA, USA) were tested: Biomed White Resin, Surgical Guide Resin, Elastic 50A V1, and Biomed Elastic 50A. Samples were 3D-printed in-house as 30 x 30 x 5 mm squares using the Form 3B SLA printer. Post-processing was carried out per manufacturer instructions to ensure complete polymerization and removal of residual monomers, including washing in isopropanol with a Form Wash tank, followed by post-curing in a Form Cure chamber. Biomed White Resin and Surgical Guide Resin samples were sanded using progressively finer grit sizes ranging from 200 to 800 to achieve a smooth, uniform surface finish. The final 3D-printed candidates are presented in **Figure 0-1.** All 3D-printed material candidates tested for their material properties.

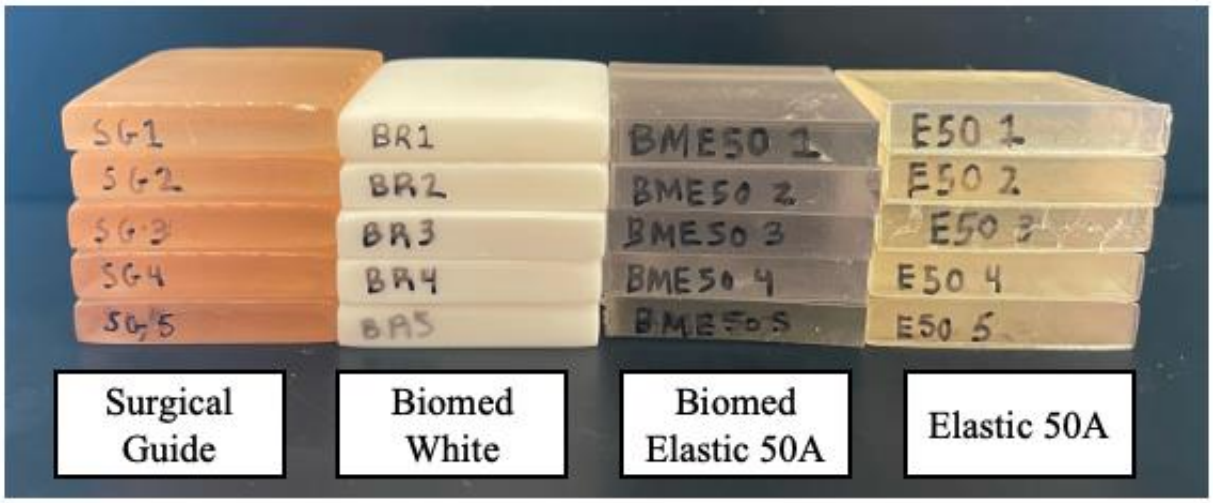

Figure 0-1. All 3D-printed material candidates tested for their material properties.

The experimental setup for materials properties testing is shown in **Figure 0-2..** A custom-built 3 MHz single-element transducer was mounted on a positioning system and submerged in a tank filled with degassed, deionized water. A high-sensitivity rod hydrophone (HNR-0500, Onda Corp., Sunnyvale, CA, USA) was mounted on the positioning system, with the rod tip oriented toward the transducer face. The hydrophone output was connected to a digital oscilloscope which captured the voltage waveforms corresponding to the acoustic signals. A MATLAB code was used to convert the recorded voltage waveforms into pressure values (MPa) using the hydrophone's sensitivity calibration. The acoustic focus was located approximately 75 mm from the transducer surface. After identifying the focus, the hydrophone was moved in the x-direction into the far field (~120 mm) to obtain a more stable and reliable measurement of the sound field.

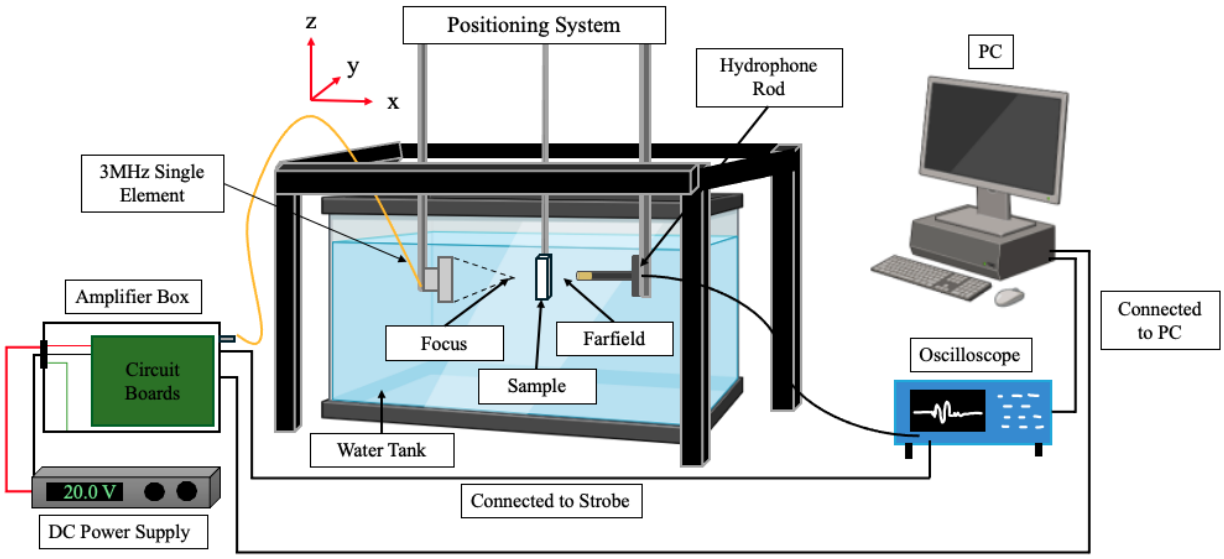

Figure 0-2. Experimental setup for material properties testing. A 3 MHz single-element transducer and a high-sensitivity rod hydrophone were mounted on a positioning system in degassed, deionized water. Acoustic signals were recorded via a digital oscilloscope and converted into pressure values (MPa) using MATLAB. The hydrophone was first positioned at the acoustic focus (75 mm) and then moved axially to the far field approximately 120 mm beyond the focus, resulting in a total distance of 195 mm from the transducer.

Each sample was individually mounted in a custom 3D-printed holder between the 3 MHz transducer and the rod hydrophone, ensuring alignment with the hydrophone tip. The hydrophone was fixed 195 mm from the transducer, while samples were positioned at 150 mm and, for comparison, at 100 mm away from the transducer to confirm consistent alignment and measurement performance. A control waveform was first recorded using the empty holder, followed by waveforms for each sample type at an input of 20 V. For each material, five replicates (n = 5) were tested to account for variability and ensure reliable measurement of acoustic properties. Sample dimensions were measured with a caliper, and mass was recorded with a laboratory precision balance for input into the MATLAB script provided in **Appendix B**. Acoustic Impedance and Sound Speed Matlab Code**.** This script calculated sound speed and acoustic impedance using the time-of-flight difference between the control and sample waveforms. A separate MATLAB code was used to determine acoustic attenuation for each material, as detailed

in **Appendix C.** Attenuation Matlab Code The script included frequency domain analysis with adjustable limits to extract peak magnitudes around 1, 2, and 3 MHz. These values were then plotted in Excel, and the slope of a linear regression model was used to calculate the attenuation of the material in units of dB/cm/MHz.

3.2.2 ISO 10993 Biocompatibility: Cytotoxicity Test

The cytotoxicity evaluation of 3D-printed samples was conducted in accordance with ISO 10993-5:2009 to assess potential toxic effects of material extracts on cultured mammalian cells [3]. The experimental workflow is summarized in **Figure 0-3.**. The same four *Formlabs* resins were tested, along with an additional material, Advanced HighTemp PerFORM from Proto Labs (Maple Plain, MN, USA). *Formlabs* samples were prepared using the same in-house 3D-printing and post-processing procedure described in Section 3.3.1. Sterilization methods varied by material, as required for cytotoxicity testing under ISO 10993-5 to ensure that biological responses reflect the material itself rather than contamination [3]. Following the manufacturer's technical sheet, Biomed White, Surgical Guide, and HighTemp PerFORM resins were autoclaved at 121°C for 30 minutes, while Elastic 50A V1 and Biomed Elastic 50A were sterilized by soaking in 70% ethanol for 5 minutes, rinsing with ultrapure water, and allowing them to dry under laminar airflow (Class II biosafety cabinet) before extraction.

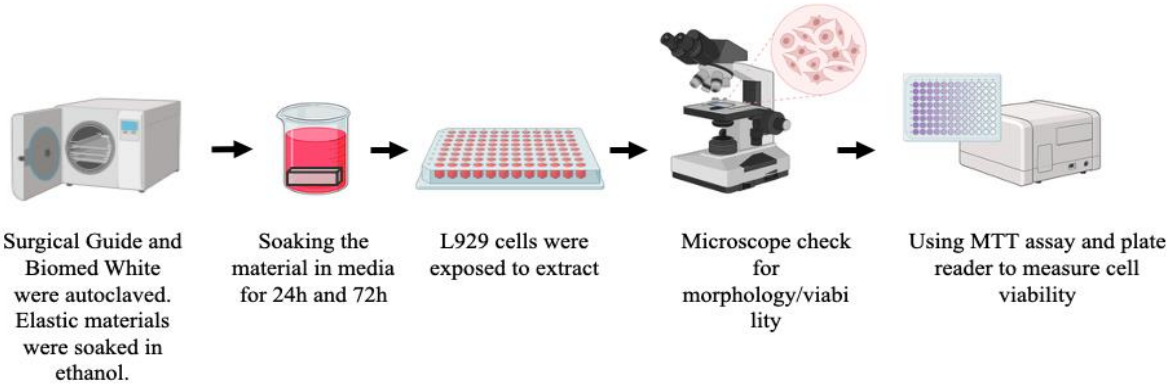

Figure 0-3. The workflow for cytotoxicity testing includes extraction of 3D-printed materials, application of extracts to L929 cells, microscopic observation, and assessment of cell viability using the MTT assay and microplate reader.

The cell line used in this experiment was mouse fibroblast L929 cells (ATCC, VA, USA), as recommended by ISO 10993-5 for cytotoxicity testing [3]. Cells were cultured in 75 cm^2 tissue culture flasks and maintained at 37°C under 5% CO_2 in complete Dulbecco's Modified Eagle Medium (DMEM) supplemented with 10% fetal bovine serum (FBS) and 1% Penicillin-Streptomycin to support cell growth and prevent contamination. Once the cells reached 70–80% confluency, they were harvested using trypsinization, stained with Trypan Blue to assess viability, and counted using a hemocytometer. Two 96-well plates were prepared separately one designated for the 24-hour extract incubation and the other for the 72-hour extract incubation. Cells were seeded into each plate at a density of 1×10^4 cells per well in 100 µL of complete medium and incubated for 24 hours to allow cell attachment and monolayer formation. Following this period, the medium was carefully aspirated, and 100 µL of the prepared sample extracts were added to each well. The plates were then incubated for an additional 24 hours to allow exposure to potential cytotoxic effects. A negative control (complete culture medium) and a positive control (2% Triton X-100) were included for comparison. Each experiment was performed with n = 5 replicates.

Cell viability was qualitatively assessed using a microscope and quantitively assessed using the MTT (3-(4,5-dimethylthiazol-2-yl)-2,5-diphenyltetrazolium bromide) colorimetric assay (CyQUANT MTT Cell Viability Assay, Themo Fisher Scientific, Waltham, MA, USA) which measures mitochondrial reductase activity in viable cells. After the exposure period, the test extracts were removed and each well received 100 µL of fresh DMEM followed by 10 µL of MTT solution (5mg/mL in PBS). The plates were wrapped in aluminum foil to protect them from light and incubated at 37°C under 5% CO_2 for 4 hours to allow formazan crystal formation. Following incubation, the MTT-containing medium was carefully aspirated, and 100 µL of dimethyl

sulfoxide (DMSO) was added to each well to dissolve the formazan crystals. Wells were gently pipetted to ensure thorough mixing while minimizing bubble formation. The absorbance of the resulting purple solution was measured at 540 nm using a SpectraMax iD3 microplate reader (Molecular Devices, San Jose, CA).

3.2.3 IEC 60601-1 Electrical Safety Testing

All electrical safety tests were performed in accordance with IEC 60601-1 using a calibrated OMNIA II 8206 Electrical Safety Analyzer (ESA) (Associated Research, Lake Forest, IL, 60045). The ESA has incorporated standardized Measuring Devices (MD) to simulate human body electrical characteristics, ensuring clinically relevant leakage current evaluations [5]. Tests were performed under both normal condition (NC) and single-fault condition (SFC) to validate the medical device's safety under expected use and potential failure scenarios. All leakage current tests were conducted at 110% of the rated voltage to account for potential voltage fluctuations during operation, ensuring that the device's electrical safety is maintained even under conditions that may exceed the nominal voltage during normal operation [4]. A variable transformer was integrated into the leakage test setups to precisely adjust the input voltage to 110% of the device's rated supply volage. All parameters for each test on the ESA are shown in **Appendix D.** Electrical Safety Analyzer Parameters

The protective earth (ground) bond test illustrates the test setup in **Figure 0-4**. The test verifies the integrity of the grounding path by applying a high current of 25A between the protective earth terminal and all accessible conductive parts of the Device Under Test (DUT). The test used a 6 V current source with a 5-second dwell time, ensuring compliance with the <100 mΩ limit as specified in clause 8.6.4 of IEC 60601-1 [4]. **Figure 0-5** shows a schematic where

current is applied through the line terminal and returned via the protective earth path to confirm the continuity and low resistance of the grounding connection.

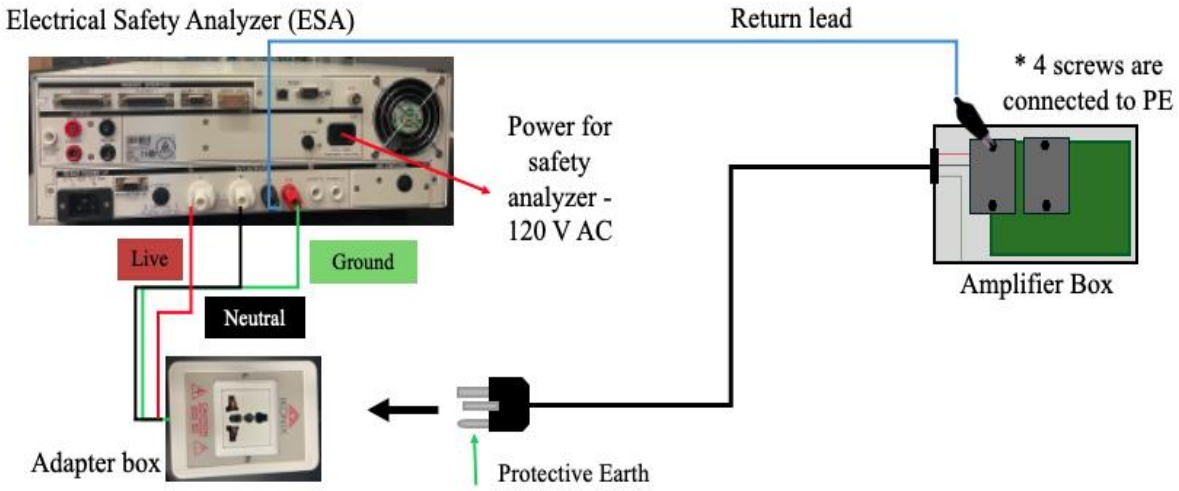

Figure 0-4. This figure illustrates the ground bond test procedure where the ESA supplies power to the amplifier (DUT), causing current to flow through the protective earth conductor of the DUT The return current passes through the conductive parts of the DUT (metal screws) and returns via the return lead to the ESA, which measures the resistance of the protective earth path to ensure it meets safety standards.

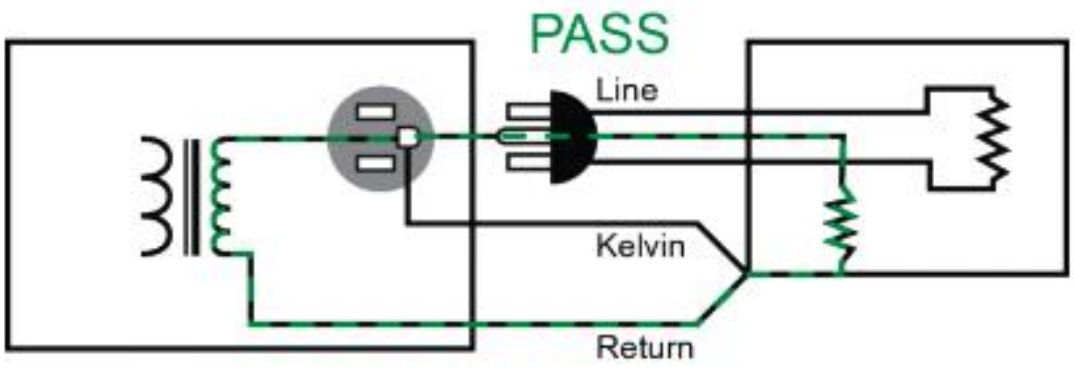

Figure 0-5. Adapted from "3 Ways to Simplify Medical Device Testing," HIK Consulting [6]. Ground bond test configuration measuring continuity between the power plug ground pin and the device chassis

The earth leakage current test (**Figure 0-7**) measures the current flowing through the insulation to the protective earth conductor in Class I medical devices with Types B, BF, or CF applied parts. **Figure 0-6** shows the schematic used during this test, where the analyzer applies current to the DUT and measures any leakage returning through the ground path to the device

chassis. Testing is conducted under three key conditions: normal operation, reverse operation, and a SFC where the neutral conductor is open-circuited. The test excludes "open earth" fault conditions as these would invalidate the measurements. Earth leakage current was measured with test limits of ≤ 5 mA (NC) and ≤10 mA (SFC) [4]. This test does not apply to Class II (double-insulated) devices.

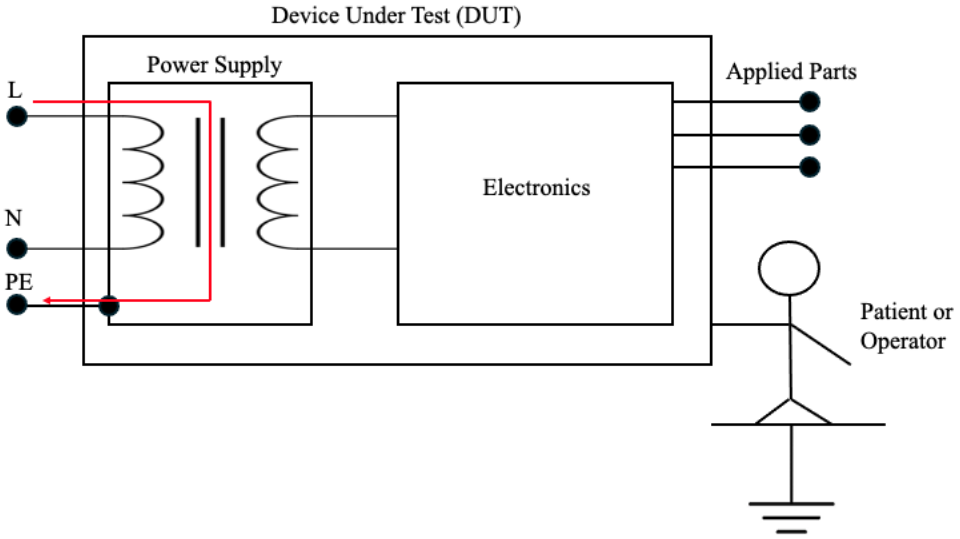

Figure 0-6. Earth leakage test schematic showing how the analyzer applies current to the DUT and measures leakage through the ground path to the device chassis.

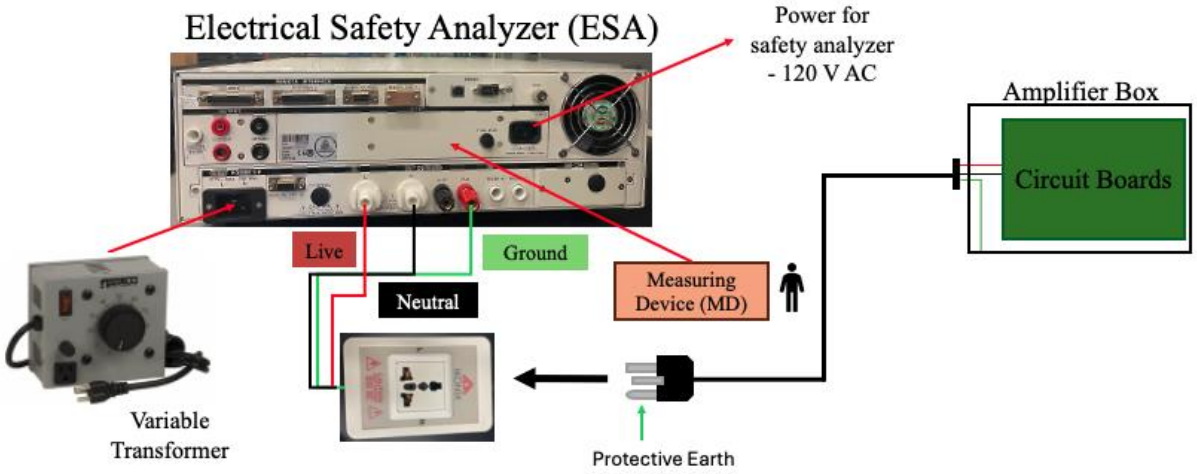

Figure 0-7. This figure illustrates the Earth Leakage Test procedure, where the ESA supplies power to the amplifier (DUT) through a variable transformer to enable testing at 110% of the rated voltage, as required by IEC 60601-1 [4]. Current flows through the DUT, and the return current passes through the MD, which simulates human body impedance. The ESA then measures any

leakage current flowing through the protective earth, ensuring compliance with test limits of ≤ 5 mA (NC) and ≤10 mA (SFC) [4].

The single-touch enclosure leakage current test evaluates the unintended current that may flow from accessible conductive parts of medical electrical equipment through a simulated patient or operator to ground. **Figure 0-8** illustrates the schematic used for this test, where the analyzer simulates a single fault condition and measures the current flowing from the device enclosure to ground. The single-touch enclosure leakage current test (

Figure 0-9) is performed under normal conditions (NC), reversed polarity, and several single fault conditions (SFC), including open neutral, open ground, open ground with reversed polarity, and open neutral with reversed polarity. As specified in IEC 60601-1, if the DUT is made entirely of insulating material, a 10 × 20 cm conductive foil may be placed on the enclosure to serve as a probing point [4]. Leakage current is measured through the measuring device (MD) connected between each accessible part and earth, with compliance limits of ≤100 µA under NC and ≤500 µA under SFC [4].

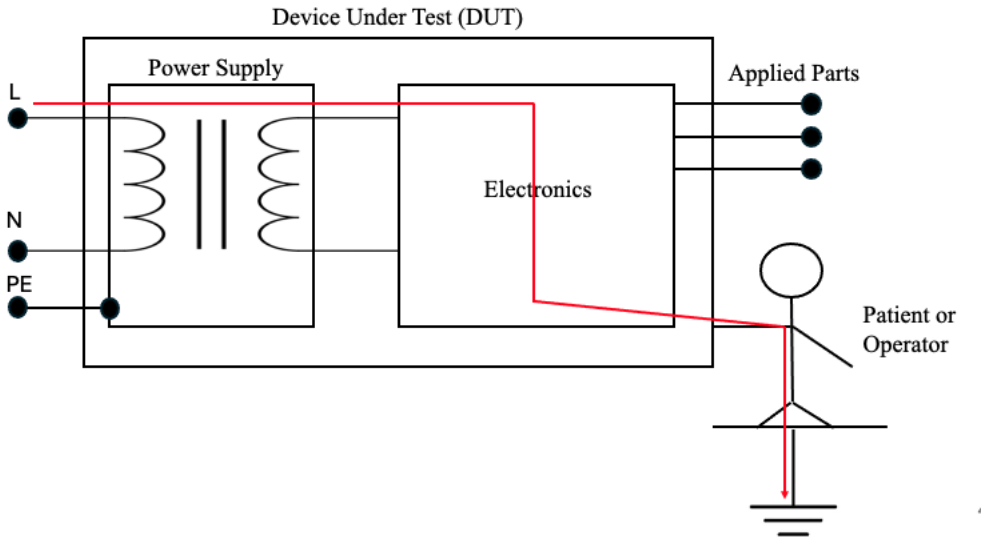

Figure 0-8. Single-touch enclosure leakage current test schematic illustrating how the analyzer simulates a single fault condition and measures current flowing from the device enclosure to ground through a simulated patient or operator touch.

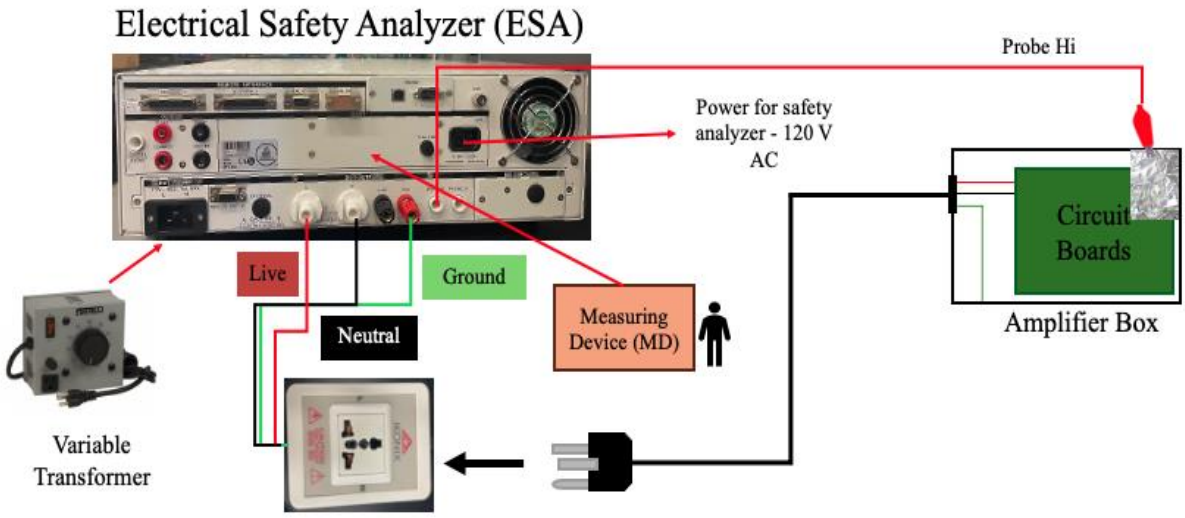

Figure 0-9. This figure illustrates the test setup for measuring single-touch enclosure leakage current. The ESA supplies power to the amplifier (DUT) through a variable transformer, which allows testing at 110% of the rated voltage as required by IEC 60601-1 [4]. Current flows through the DUT, with any leakage current returning through the high probe and passing through the MD, which simulates human body resistance. The ESA then measures the current leaking through the enclosure to ensure compliance with limits of ≤100 µA (NC) and ≤ 500 µA (SFC) [4].

The two-touch enclosure leakage current test assesses the risk posed when a patient or operator simultaneously contacts two different conductive surfaces on the device, potentially completing a current path through the body. **Figure 0-10** illustrates the schematic setup for this test, showing how current is measured between two accessible conductive parts to simulate a fault condition without using an earth reference. The two-touch enclosure leakage current test (**Figure 0-11**) uses the same test conditions as the single-touch test: normal conditions (NC), reversed polarity, and single fault conditions (SFC). Leakage current is measured between two points on the DUT. One probe is connected to a 10 × 20 cm conductive foil placed on one accessible part, and the other to foil on a different part [4]. This setup simulates simultaneous contact by a user. The test follows the same leakage current limits as the single-touch test, with ≤100 µA under NC and ≤500 µA under SFC, in accordance with IEC 60601-1 [4].

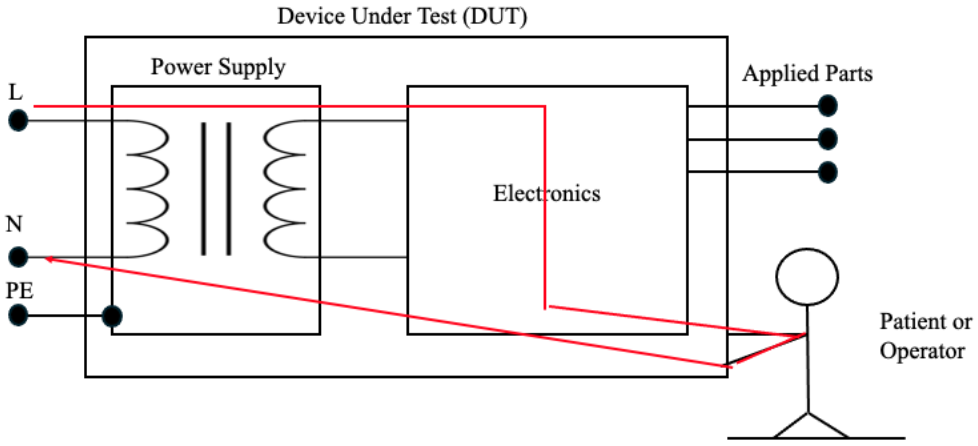

Figure 0-10. Two-touch enclosure leakage test schematic showing current measurement between two simultaneously accessible conductive parts, simulating a potential path through a patient or operator under a fault condition.

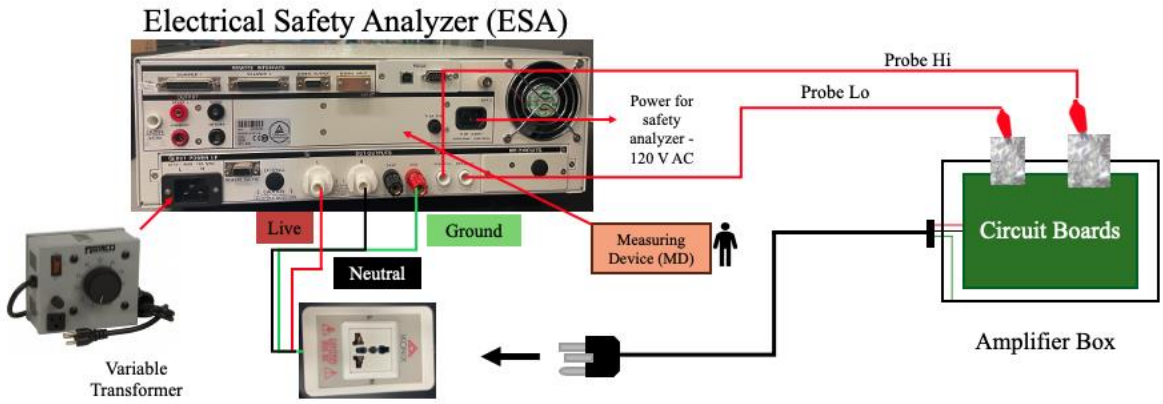

Figure 0-11. This schematic demonstrates the test setup for measuring two-touch enclosure leakage current. The ESA supplies power to the amplifier (DUT) through a variable transformer, enabling testing at 110% of the rated voltage [4]. As current flows through the device, any leakage current from the enclosure is detected as it flows from Probe Hi to Probe Lo, passing through the MD, which simulates human body impedance. The ESA then measures the leakage current to ensure compliance with IEC 60601-1 limits of ≤100 µA under normal conditions (NC) and ≤500 µA under single-fault conditions (SFC) [4].

The patient leakage current test evaluates potential electrical risks when patients come into contact with applied parts of medical devices, such as FUS transducers. **Figure 0-12** shows the schematic used for this test, where current is measured from the applied parts through a simulated patient pathway to ground under both normal and fault conditions. **Figure 0-13** displays the

physical test setup, illustrating how the transducer, saline solution, and measurement device are arranged during testing. According to IEC 60601-1, applied parts may be classified as Type B, BF, or CF based on their intended use, electrical connectivity, and proximity to the heart [4]. Type B parts are not functionally conductive and can be quickly removed from the patient [4]. Type BF parts may have conductive elements and must be electrically isolated from ground for safe use in non-cardiac applications [4]. Although the FUS transducers used in this study have non-conductive housings and no exposed metal, they contain internal electronics and are intended for prolonged patient contact. As such, they would most likely be classified as Type BF applied parts, since damage to the housing could expose internal conductors, place the patient at ground potential, and cause the device to fail BF safety requirements. According to IEC 60601-2-62, high-intensity therapeutic ultrasound devices must be tested in a 0.9% saline solution to accurately simulate the human body's physiological conditions [7]. This test is conducted at 110 % of the rated voltage using a measuring device that simulates patient impedance. The test verifies compliance with strict leakage limits of ≤100 μA during normal conditions and ≤500 μA under single fault conditions [4]. It is performed under normal conditions and reversed polarity, as well as single fault conditions including open neutral, open ground, open ground with reversed polarity, and open neutral with reversed polarity.

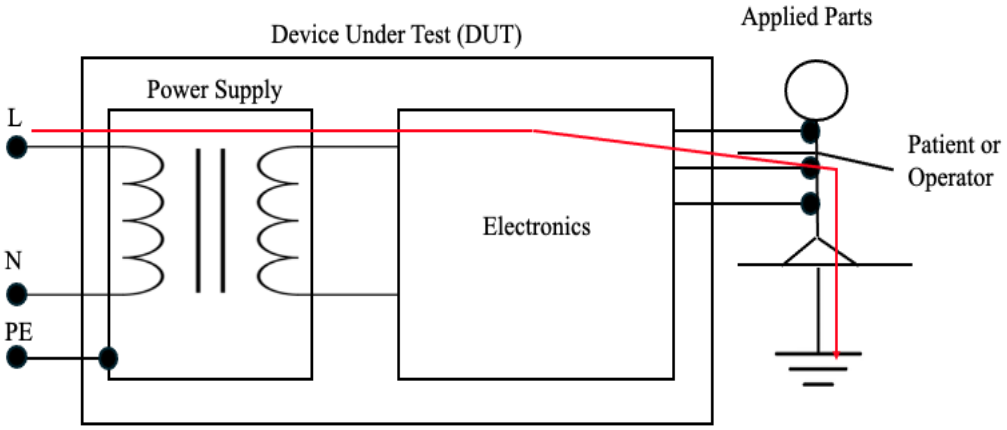

Figure 0-12. Patient leakage current test schematic showing how current is measured from the applied parts through the simulated patient pathway to ground, assessing leakage under normal and single fault conditions.

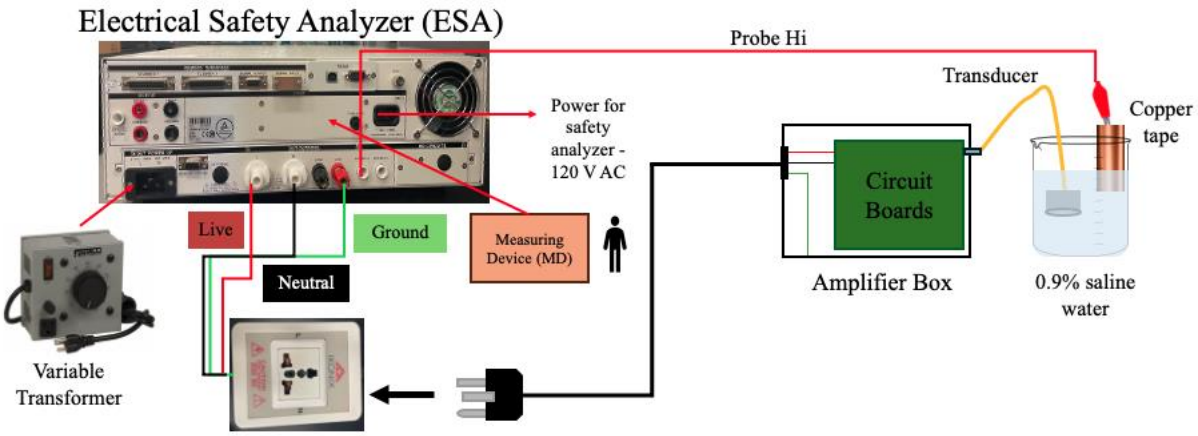

Figure 0-13. This figure illustrates the test setup for measuring patient leakage current. The ESA, powered through the variable transformer, supplies power to the amplifier (DUT), and current flows from the transducer through the 0.9% saline water to the copper tape, which acts as a conductive path. Return current flows from Probe Hi through the MD. The ESA then checks for any current leaking through the transducer, ensuring compliance limits of ≤100µA during NC and ≤500µA under SFC [4].

3.2.4 Single Element Construction

Biocompatible 3D printed resins including Surgical Guide, Biomed White, and Biomed Elastic 50A were printed in house to fabricate acoustic housings for single-element transducers. The construction of these 3MHz single elements is the same as the ones usually built in-house but

with a different material for the housing. Prior to assembly, 3 MHz Pz36 disc piezoelectric (Ferroperm Pz36, low acoustic impedance PZT, Meggitt A/S, Coventry, UK) were cleaned with isopropanol. Two wires, one positive and one negative, were soldered to opposite ends of the face of the Pz36 disc. Both faces of the disc and the inner surfaces of the printed lens housings were primed by dabbing 1:1 solution of Chemlok AP-121 and 200-proof ethanol and were allowed to sit for 10 minutes. Loctite E-120HP Hysol epoxy (Henkel Corporation, Rocky Hill, CT, USA) was then applied to the inner surface of the lens housing, and the Pz36 disc was carefully pressed in, first on one side, then the other, to eliminate trapped air between interfaces. A weight of approximately 450 grams was placed on each element pressing the down the Pz36 disc and left to cure overnight. After curing, the backing of each element was threaded through a BNC cable. The cable end was stripped approximately one inch, and the outer blue protective foil layer was removed to expose the woven copper shield. The shield was twisted together, and the inner insulation was stripped to expose the conductor. The central wire was soldered to the positive terminal of the Pz36, while the twisted shield was connected to the negative terminal (ground). The backing was then slid slightly up the BNC cable and bonded to the rim of the printed lens using 5-minute epoxy, followed by a coating of Plasti Dip (Plasti Dip International, Blaine, MN, USA) for additional sealing. Plasti Dip was also applied around the cable entry point on the backing to prevent any potential water ingress and protect the internal components.

3.2.5 IEC 62127-1: Acoustic Characterization

A total of four single-element transducers were characterized: three biocompatible 3 MHz elements fabricated as described in Section 3.3.4, and one standard 3 MHz transducer with a PerFORM housing, which serves as a commonly used reference device in the lab (n = 1). The experimental setup followed the same configuration used for material property testing in Section

3.3.1. Each transducer was submerged in a degassed, deionized water tank, and both the transducer and a calibrated rod hydrophone were mounted on a 3-axis positioning system, with the hydrophone tip aligned to face the surface of the transducer. Acoustic field measurements were conducted in accordance with IEC 62127-1, which outlines procedures for characterizing ultrasound fields using hydrophones [8]. The hydrophone was positioned at the acoustic focus of the transducer, and pressure waveforms were acquired over a 5.5 × 5.5 mm grid in the yz-plane using a step size of 0.25 mm, resulting in a 45 x 45 point grid (2025 measurement locations). This step size was chosen to provide sufficient spatial resolution of the beam profile. At 3 MHz, the wavelength of ultrasound in water is approximately 0.5 mm, and a step size equal to half the wavelength meets the Nyquist criterion for spatial sampling, ensuring that key features of the acoustic field, such as focal peak pressures and beam symmetry, are accurately captured [8].

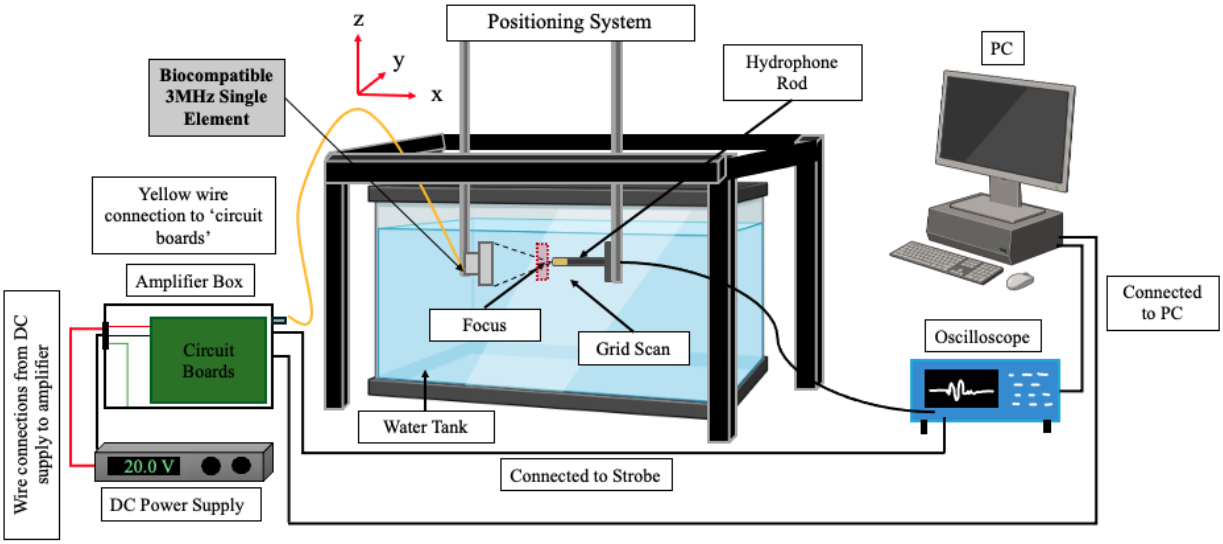

Figure 0-14. Experimental setup for grid scanning of the acoustic field using a 3 MHz single-element transducer and a high-sensitivity hydrophone.

All MATLAB codes used for these calculations are provided in **Appendix** E. I_{SPTA} and I_{SPPA} Matlab Code**E**. The collected pressure data were processed in MATLAB to calculate the following acoustic intensity metrics for each transducer:

Pulse Duration: To calculate the pulse duration according to IEC 62127-1, each pressure waveform was first squared, representing the instantaneous acoustic energy [8]. The squared pressure was then integrated over time to generate a cumulative energy curve. The time points at which the cumulative energy reached 10% and 90% of its final value were identified as t_{10} and t_{90} respectively. The pulse duration was calculated using Eq 3.1:

$$t_d = 1.25\,(t_{90} - t_{10}) \qquad [Eq.\,3.1]$$

This energy-based method offers a consistent metric for pulse duration. An example of the pulse duration calculation is shown in **Figure 0-15** with the 10% and 90% energy points indicated directly on the pressure waveform.

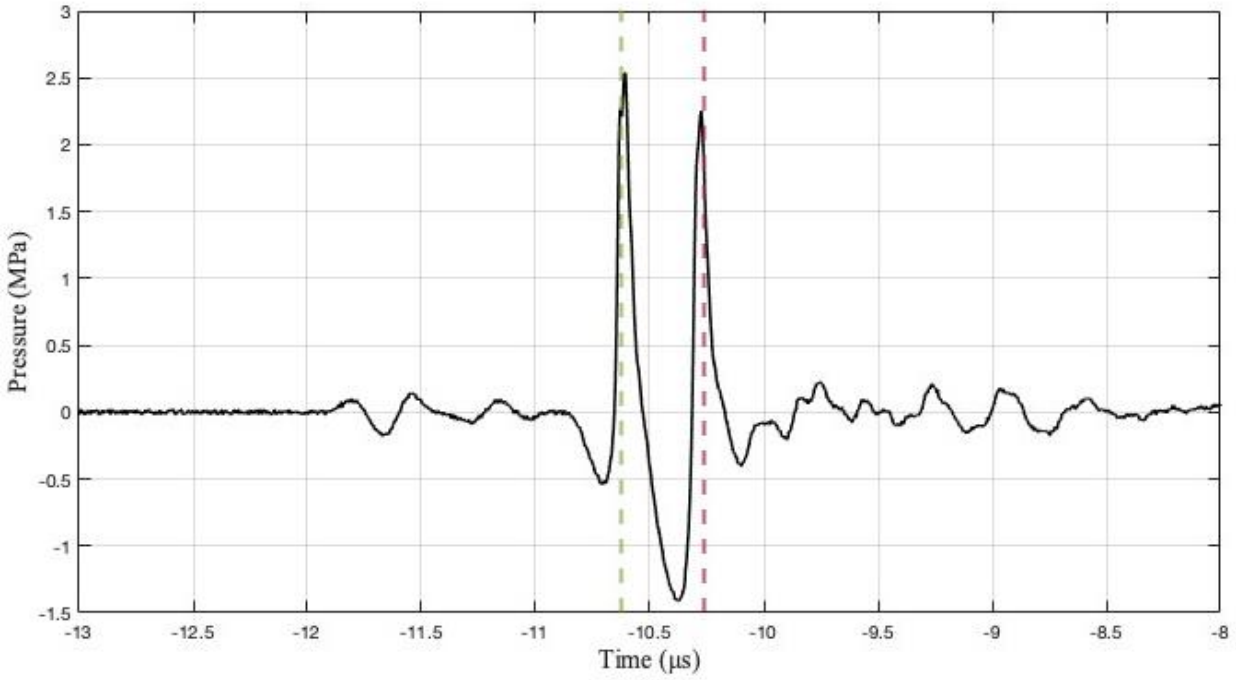

Figure 0-15. A representative pressure waveform used to calculate pulse duration. The time points where the squared pressure waveform reaches 10% (green) and 90% (red) of its total energy are marked, and the interval between them is used to determine the pulse duration.

I_{SPPA}: For each of the 2025 grid points, the instantaneous acoustic intensity was calculated shown below in Eq.3.2:

$$I(t) = \frac{p(t)^2}{\rho\, c} \qquad [Eq. 3.2]$$

where p(t) is the pressure waveform in pascals, ρ is the density of the medium (1000 kg/m³ for water), and c is the speed of sound (1500 m/s). The pulse-average intensity was then calculated by averaging the instantaneous intensity I(t) over the pulse duration, t_d demonstrated in **Figure 0-16**. Finally, I_{SPPA} is determined by identifying the maximum pulse-average intensity across all grid points in the measurement plane. The equation for I_{SPPA} from IEC 62127-1 is shown in Eq. 3.3 [8].

$$I_{SPPA} = \frac{1}{t_d \rho c} \int p^2(t)dt \qquad [Eq. 3.3]$$

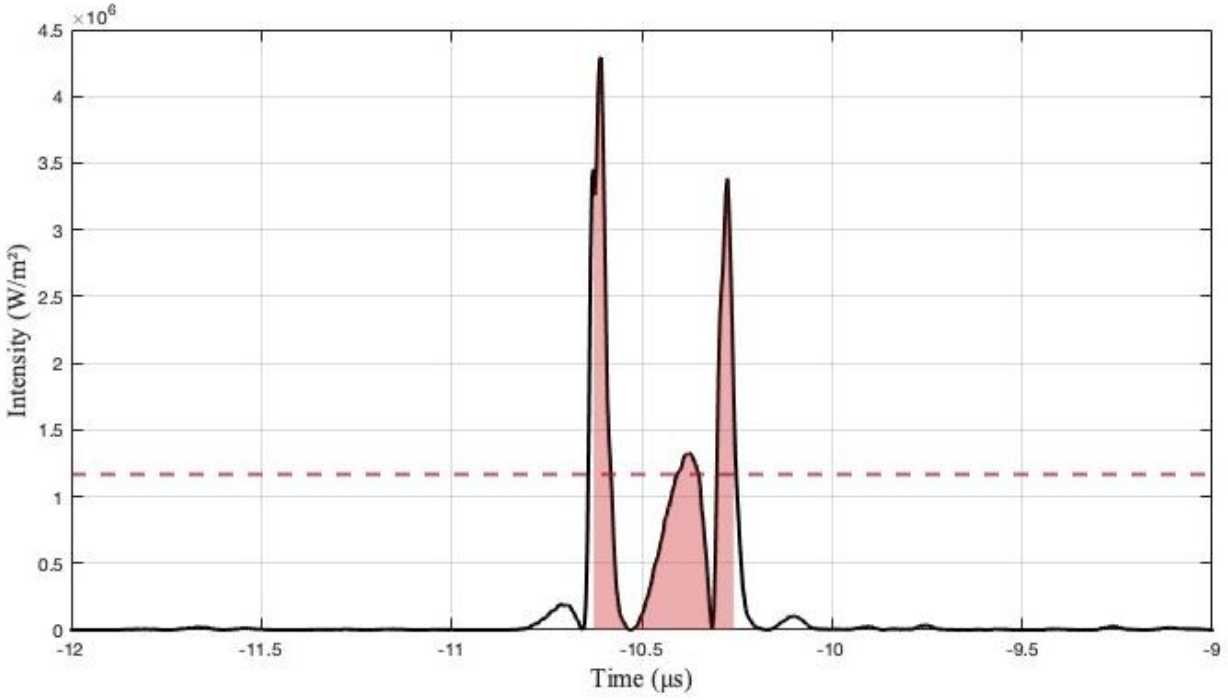

Figure 0-16: The red shaded area highlights the part of the pulse (i.e. the pulse duration) used to calculate pulse average intensity. The red dashed line marks the peak of this average intensity across all grid points, which is reported as I_{SPPA}.

I_{SPTA}: Spatial-peak temporal-average intensity was calculated at each of the 2025 grid points using the pressure waveform data. At each point, the pressure waveform was squared and integrated over the duration of a single pulse. The maximum value from the integrated squared pressure was then multiplied by the pulse repetition frequency (PRF) and divided by the acoustic impedance of the medium (ρc), following the equation shown in Eq. 3.4. This accounts for both the strength of each pulse and how often pulses are repeated, including the quiescent periods between them. The spatial peak I_{SPTA} was then taken as the highest value across all grid points. This provides a measure of the average energy being delivered over time at the point of maximum intensity.

$$I_{SPTA} = \frac{PRF}{\rho c} * \max \int p^2(t)dt \qquad [Eq. 3.4]$$

3.3 Results

3.3.1 Acoustic Properties of 3D-Printed Resins

The acoustic material properties of candidate 3D-printed resins were characterized, including sound speed, acoustic impedance, and attenuation coefficient. These values were calculated using MATLAB based on time-of-flight differences obtained during the material properties testing described in section 3.3.1. Furthermore, after determining the acoustic impedance values, the attenuation coefficients were calculated using a separate MATLAB script. **Figure 0-17** present these properties for each tested resin, showing notable variations across the different materials. Among the tested resins, Surgical Guide and Biomed White exhibited higher sound speeds (2662±23 m/s and 2381±23 m/s) and acoustic impedances (3.09±0.03 MRayl and 2.85±0.04 MRayl) respectively compared to the elastic materials. In contrast, Biomed Elastic 50A and Elastic 50A demonstrated lower sound speeds (1548±4 m/s and 1742±5 m/s) and acoustic

impedances (1.64±0.01 MRayl and 1.88±0.03 MRayl). An inverse relationship was observed with attenuation coefficients, where Surgical Guide and Biomed White showed lower attenuation (3.65±0.32 dB/cm/MHz and 4.28±0.21 dB/cm/MHz) compared to the higher attenuation coefficients measured in Biomed Elastic 50A (14.32±0.28 dB/cm/MHz) and Elastic 50A (10.02±0.24 dB/cm/MHz). **Table 10** summarizes the mean values and standard deviations for all measured acoustic properties across the resin candidates, along with PerFORM, the material currently utilized in histotripsy prototypes.

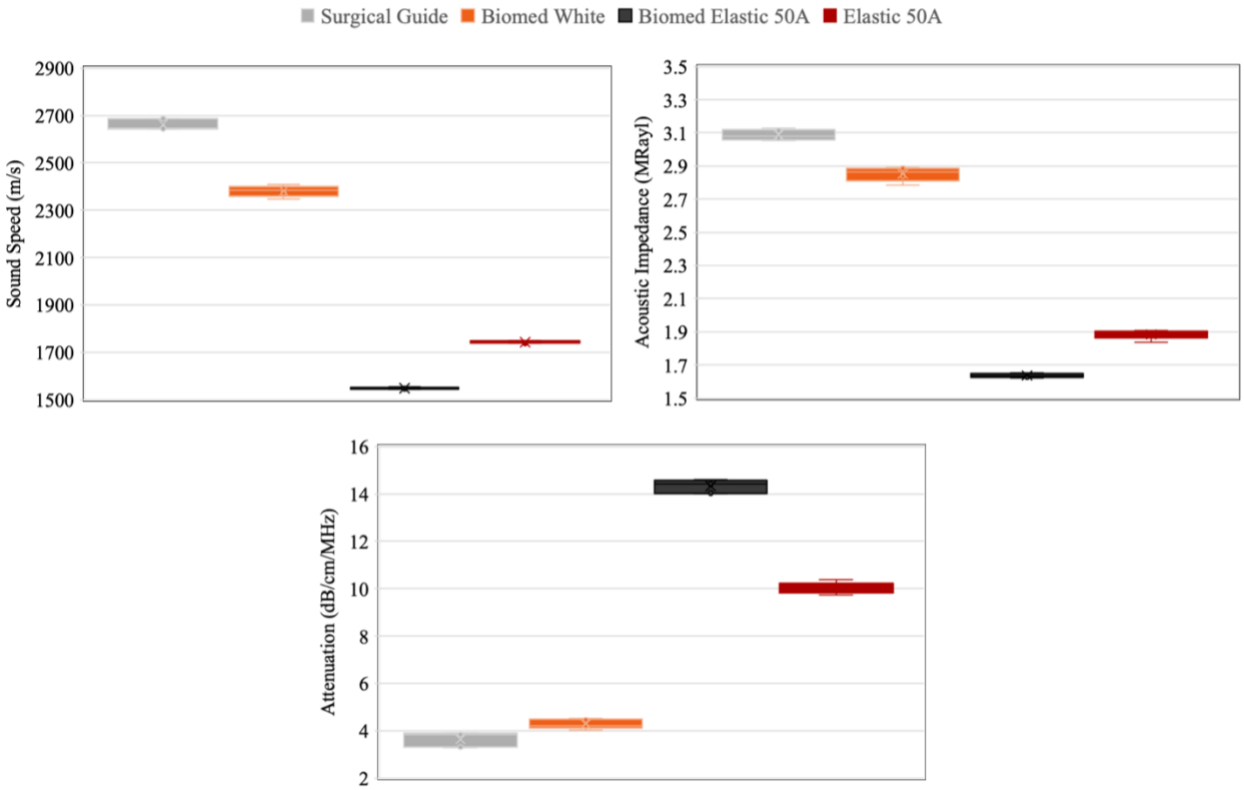

Figure 0-17. Acoustic material properties including acoustic impedance (MRayl), sound speed (m/s), and attenuation coefficient (dB/cm) calculated using MATLAB. Results are presented for each 3D-printed resin candidate.

Table 10: Mean ± standard deviation of acoustic material properties for candidate 3D-printed resins, including acoustic impedance (MRayl), sound speed (m/s), and attenuation coefficient (dB/cm).

Materials	Acoustic Impedance (MRayl)	Sound Speed (m/s)	Attenuation (dB/cm/MHz)
Surgical Guide	3.09±0.03	2662±23	3.65±0.32
Biomed White	2.85±0.04	2381±23	4.28±0.21
Biomed Elastic 50A	1.64±0.01	1548±4	14.32±0.28
Elastic 50A	1.88±0.03	1742±5	10.02±0.24
PerFORM[1]	5.12	~3500	2.39

1- Data for this material were obtained from previously conducted testing and included here for comparison purposes [9].

3.3.2 ISO 10993 biocompatibility: Cytotoxicity Test Results

The cytotoxic potential of candidate 3D-printed materials, including PerFORM, was evaluated using an MEM elution method followed by MTT assay according to ISO 10993-5 guidelines [3]. Material samples were prepared for extraction following ISO 10993-12 specifications, adhering to the required surface area to volume ratio [10]. Two separate extraction conditions were implemented: one set of samples was extracted for 24-hours and another set for 72-hours in separate containers to simulate short and long-term contact durations. The two separate condition extracts were then applied to L929 fibroblast cells, with cell viability assessed after 24h exposure through both qualitative morphological analysis and quantitative metabolic activity measurement. Untreated cells served as the negative control, while Triton X-100-treated cells served as the positive control.

Figure 0-18 presents representative cell morphology images of the materials following exposure to the 24h extraction condition. Cells exposed to the negative control exhibited normal fibroblastic morphology characterized by strong adherence and elongated with tapered ends. In contrast, positive control cells displayed clear cytotoxic effects where there is cell rounding, reduced confluency, and detachment from the flask. Qualitative assessment revealed that PerFORM extracts induced morphological changes comparable to the positive control, strongly

indicating cytotoxic potential. Biomed Elastic 50A extracts also resulted in reduced cell confluence compared to the negative control, suggesting potential biocompatibility concerns. The remaining materials (Surgical Guide, Biomed White, and Elastic 50A) produced minimal observable morphological alterations at the 24h extraction time point.

Table 11: Qualitative morphological grading scale for cytotoxicity evaluation of extracts, as defined by ISO 10993-5. Grading is based on the percentage of cell damage or detachment observed microscopically, with scores ranging from 0 (no reactivity) to 4 (severe reactivity).

Grade	Reactivity Description	Observation
0	None	No detectable cell lysis, no reduction in cell growth.
1	Slight	Few (≤20%) cells are round, loosely attached, or lysed.
2	Mild	Moderate number of cells (approximately 20–50%) showing lysis or detachment.
3	Moderate	Severe effect on cell layers with about 50-70% of cells affected.
4	Severe	Nearly complete destruction (>70%) of cell layer.

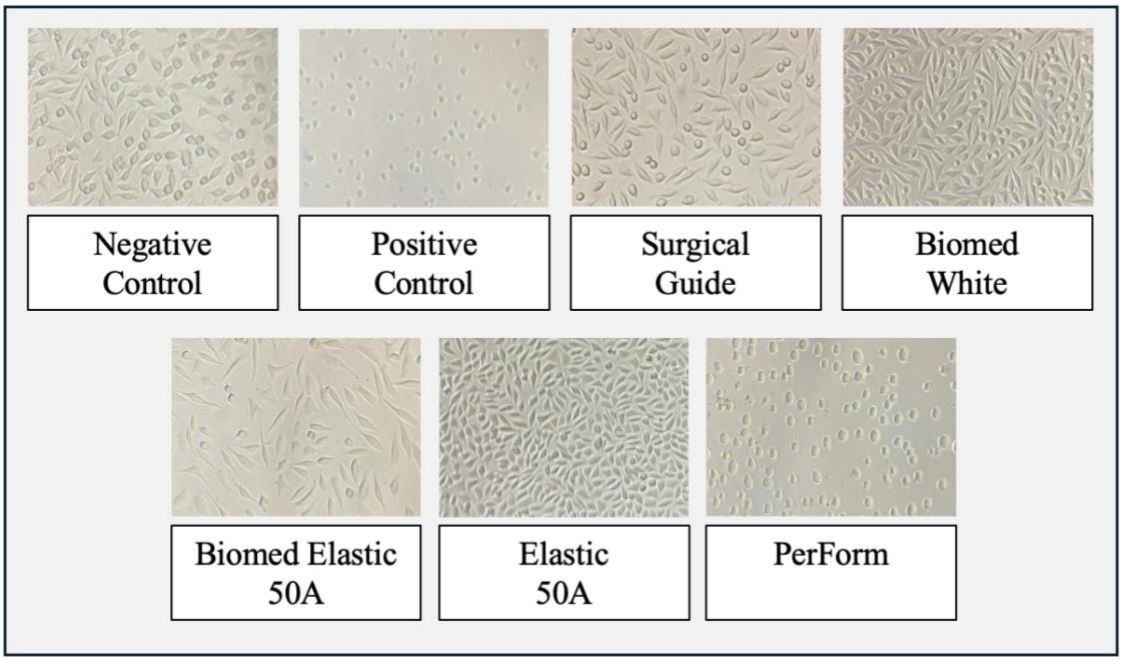

Figure 0-18. Cell morphology images taken following 24h extract exposure to 3D-printed materials. Cells were visually assessed for signs of cytotoxicity, such as cell rounding, detachment, or lysis. Images include negative control (untreated), positive control (cytotoxic agent), and each test material. Images captured at 40x magnification.

To quantitively assess cytotoxicity the common practice is referring to **Table 11** beyond subjective morphological evaluation, an MTT assay was performed to measure metabolic activity. **Figure 0-19** presents the normalized cell viability values for all tested materials. At the 24h extraction condition, Surgical Guide, Biomed White, and Elastic 50A maintained cell viability above the 70% threshold typically used to indicate non-cytotoxic behavior according to ISO standards [3]. In contrast, Biomed 50A demonstrated moderate cytotoxicity, while PerFORM showed pronounced cytotoxic effects with the lowest cell viability among all materials tested. The 72h extraction condition in **Figure 0-19** revealed increasing cytotoxic potential for most materials. Only Surgical Guide maintained high cell viability, while Biomed White measured just above the 70% threshold. Notably, all elastic materials (Biomed Elastic 50A and Elastic 50A) as well as PerFORM exhibited cytotoxic effects. PerFORM consistently demonstrated the most severe cytotoxic potential across both extraction time conditions.

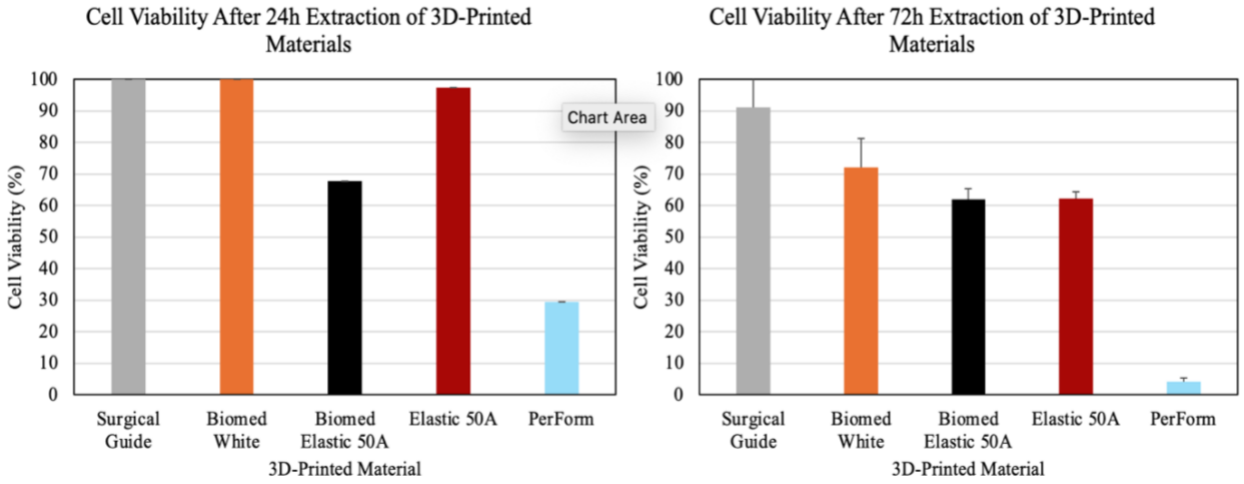

Figure 0-19. Bar graph showing percentage of cell viability for 3D-printed materials under 24-hour (left) and 72-hour extract (right) conditions. The MTT assay was performed in accordance with ISO 10993-5, with 70% viability used as the cytotoxicity threshold.

3.3.3 Electrical Safety Test Results

Electrical safety testing was performed to evaluate the device's compliance with IEC 60601-1 standards, focusing on both ground bond and leakage current assessments. All

measurements were taken using the OMNIA II 8206 Electrical Safety Analyzer, with pass/fail determinations based on specified regulatory limits. **Table 12** summarizes the ground bond test results, which assess the integrity of the protective earth connection across multiple chassis points of the device under test (DUT). The ground bond test revealed that the resistance at the top right screw of the DUT measured 103 mΩ, exceeding the maximum allowable limit of 100 mΩ. In contrast, the resistance at the top left screw was below the specified limit, indicating successful compliance for that point. However, the DUT would overall fail to meet the IEC 60601-1 requirements for protective earth resistance.

Table 12: Summary of ground bond test measurements across multiple DUT contact points. The table includes measured resistance values, the specified safety limit, and pass/fail evaluation based on compliance with IEC 60601-1 standards.

Tests	Measured Value	Limit	PASS/FAIL Status
Ground Bond Test (Top right screw)	103 mΩ	<100mΩ	FAIL
Ground Bont Test (Top left screw)	87 mΩ	<100mΩ	PASS

Table 13 presents the results for the different leakage currents tests, conducted under both normal conditions (NC) and single fault conditions (SFC). For all test types, including Earth Leakage, Enclosure Leakage, and Patient Leakage, the measured leakage currents were below the allowable limits set by IEC 60601-1 [4]. The device passed all leakage tests under both conditions.

Table 13: Summary of Leakage Test Results Under Normal Conditions (NC) and Single Fault Conditions (SFC). The table presents the measured values taken from the OMNIA II 8206 Electrical Safety Analyzer for each test type alongside their respective limits for both conditions, with pass/fail status indicated for each measurement.

Tests	Normal Conditions (NC)		Single Fault Conditions (SFC)				Limit		PASS/ FAIL Status
	NC (µA)	Reverse polarity (µA)	Open neutral (µA)	Open ground (µA)	Open ground + reverse	Open neutral + reverse	NC (µA)	SFC (µA)	

					polarity (μA)	polarity (μA)			
Earth Leakage	0.2	0.2	0.2			0.2	5000	10,000	PASS
Single touch Enclosure	0	0.3	0.5	194.4	182.6	0.6	100	500	PASS
Two touch Enclosure	0	0.2	0.4	0.7	0.6	0.4	100	500	PASS
Patient Leakage	0.4	0.4	0.5	1.6	1.6	0.5	100	500	PASS

3.3.4 Acoustic Characterization

Pressure waveforms were measured for all the biocompatible 3D-printed resins, with PerFORM serving as a control material given its established acoustic properties. **Figure 0-20** illustrates the pressure waveforms generated by each material under identical testing conditions. PerFORM exhibited the highest peak negative pressure at –1.41 MPa. Among the biocompatible resins, Surgical Guide reached –0.96 MPa, followed closely by Biomed White at –0.93 MPa. Biomed Elastic 50A demonstrated the lowest peak negative pressure at –0.20 MPa. The reduced pressures observed in the resins likely reflect differences in their acoustic or mechanical properties, such as increased attenuation or material compliance.

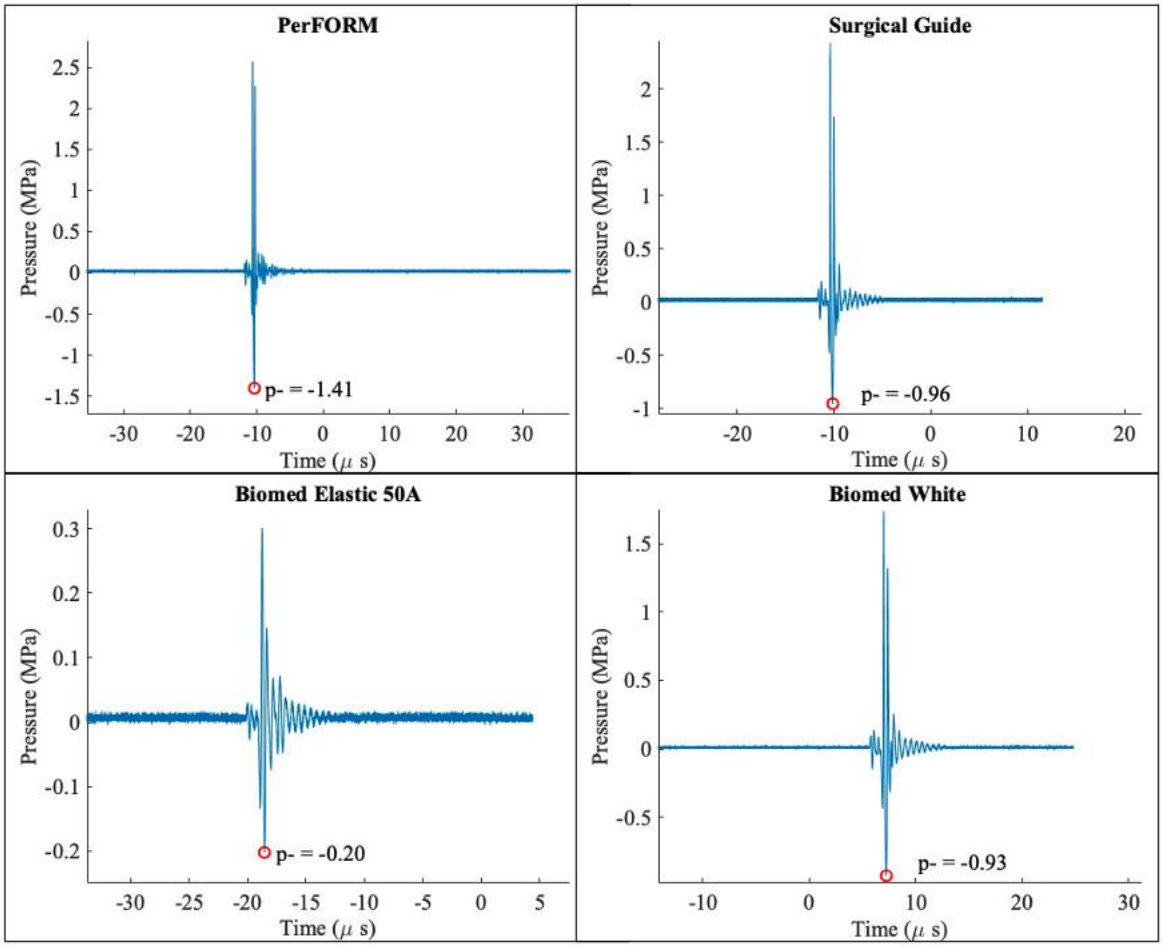

Figure 0-20. Measured pressure waveforms of biocompatible 3D printed resins and PerFORM as a control.

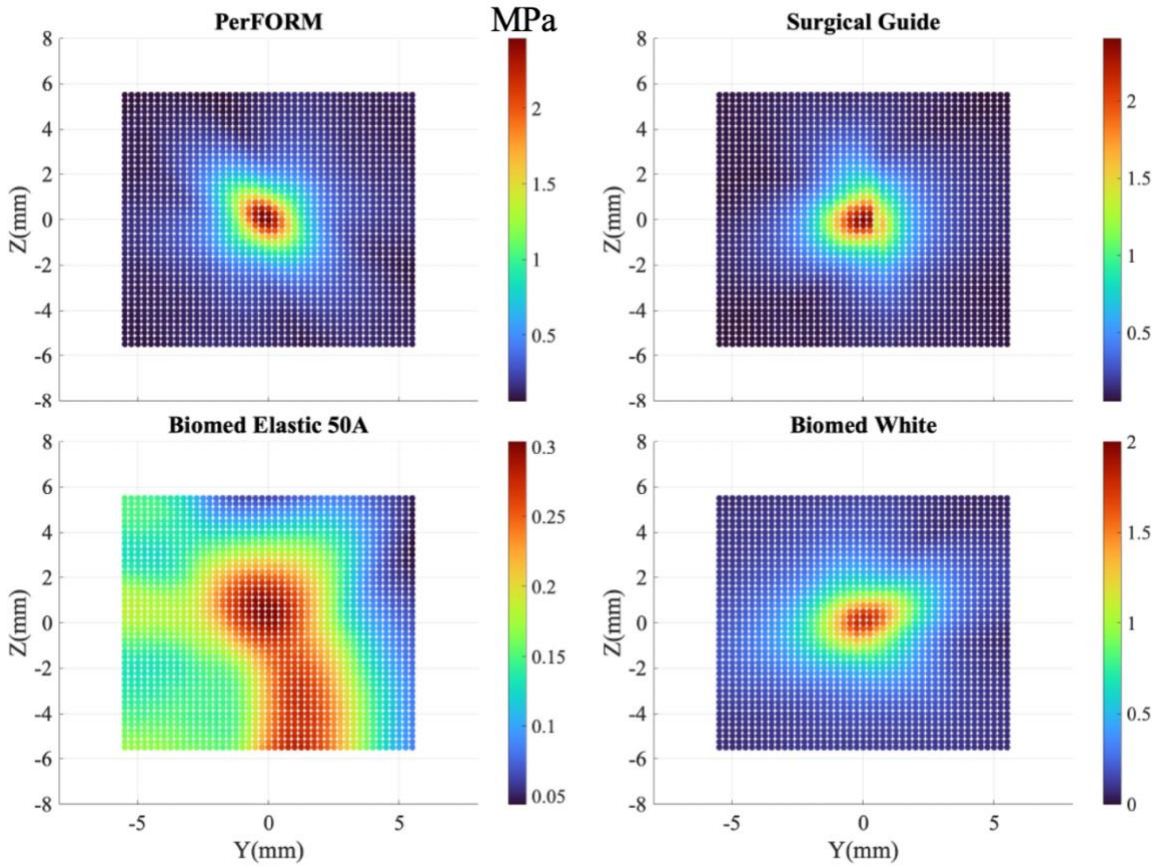

Figure 0-21. Pressure waveform grid scan of different materials acquired over a 5.5 x 5.5 mm grid in the yz-plan using a step size of 0.25 mm at the focus. The color bar indicates peak pressure values where red represents the highest peak pressure and blue represents the lowest peak pressure.

Demonstrated in

Figure 0-21, PerFORM generated a well-defined, symmetric focal spot. Surgical Guide produced a similarly focused beam with slightly reduced peak amplitude and lateral spread. Biomed White also formed a distinct focal region, though with broader spatial dispersion and reduced pressure magnitude relative to Surgical Guide. In contrast, Biomed Elastic 50A exhibited a poorly defined and irregular pressure profile, with an attenuated peak pressure below 0.3 MPa and an off-axis energy spread, indicating impaired beam focusing.

In **Figure 0-22**, PerFORM had an I_{SPPA} of 95.43 W/cm². Surgical Guide measured 56.66 W/cm², followed by Biomed White at 41.29 W/cm². Biomed Elastic 50A recorded the lowest I_{SPPA}

at 0.59 W/cm². These values reflect differences in the mechanical intensity delivered through each material under identical testing conditions.

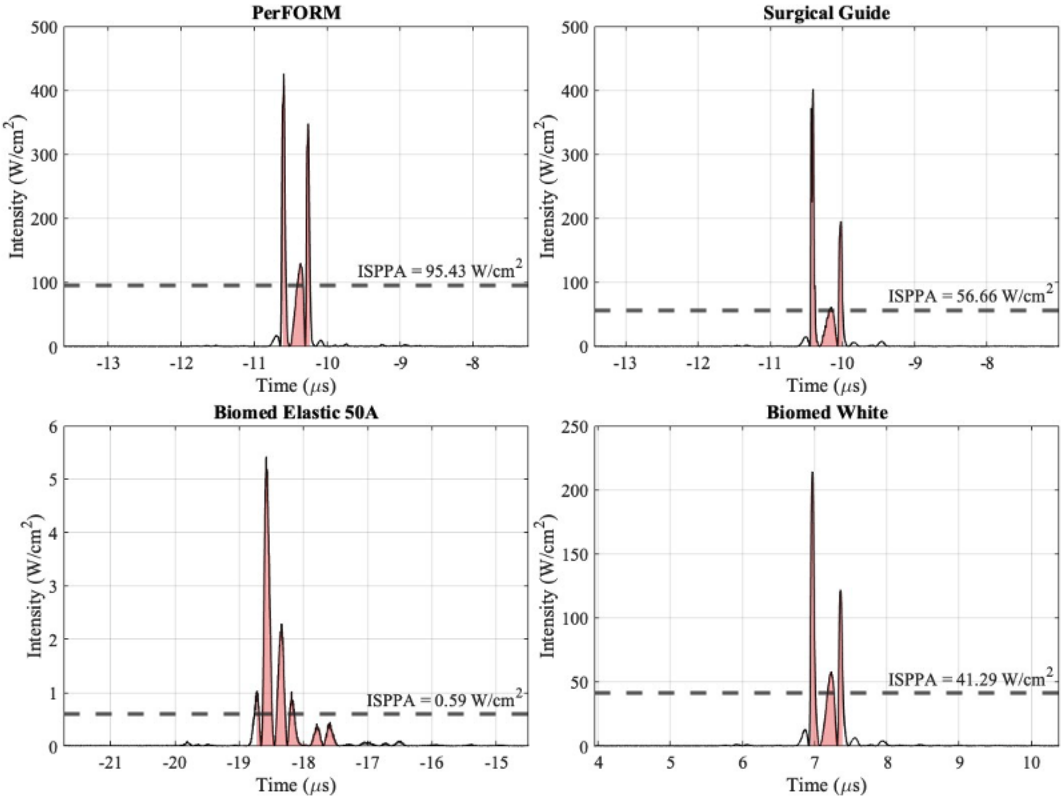

Figure 0-22. The red shaded area represents the pulse duration over which I_{SPPA} values were integrated. I_{SPPA} values are indicated by the gray dashed line for each of the four tested resins.

Figure 0-23 shows the pressure waveforms after scaling all materials to the same peak negative pressure of -30 MPa. This contrasts with **Figure 0-22**, which displays the original, unscaled waveform. When the pressure waveforms were scaled, PerFORM reached an I_{SPPA} of 44152.12 W/cm², while Surgical Guide and Biomed White reached 54413.49 W/cm² and 42617.79 W/cm², respectively. Biomed Elastic 50A exhibited a scaled I_{SPPA} of 13483.33 W/cm². Although all materials were scaled to the same peak negative pressure, variation in I_{SPPA} values remained due to differences in waveform shape and energy distribution.

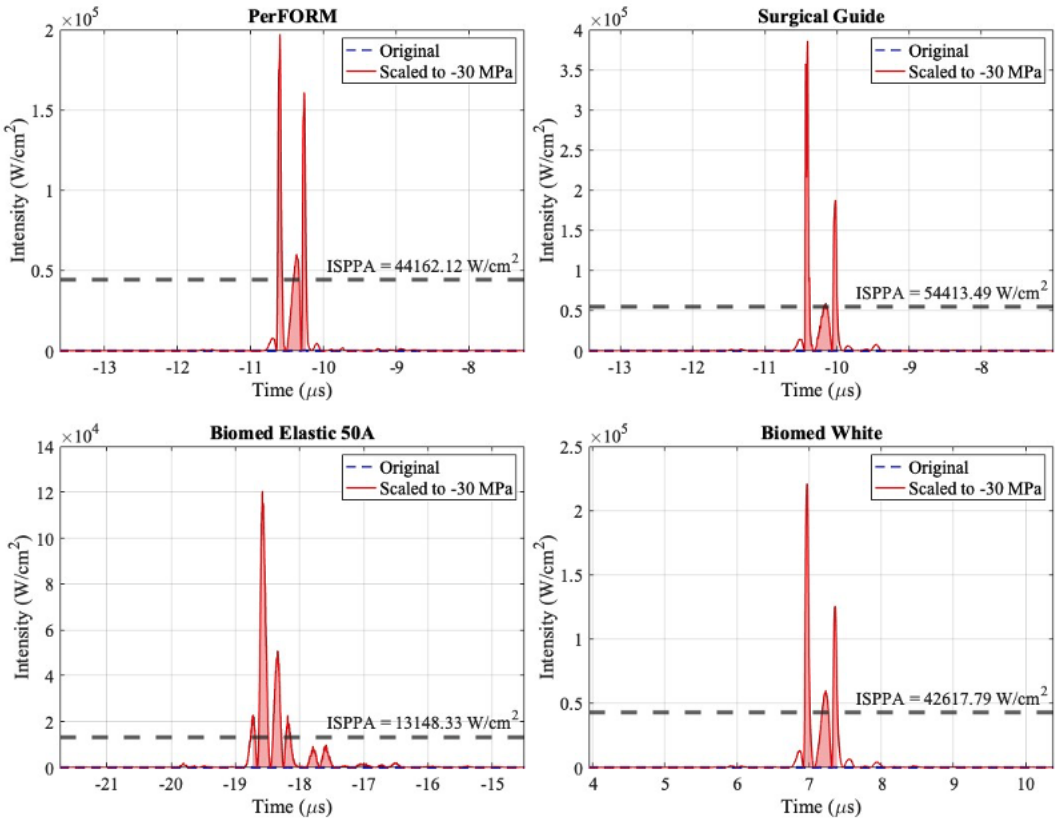

Figure 0-23. The red shaded area represents the pulse duration over which I_{SPPA} values were integrated. I_{SPPA} values for each material after scaling pressure waveforms to a peak negative pressure of -30 MPa are indicated by the gray dashed line for each of the four tested resins.

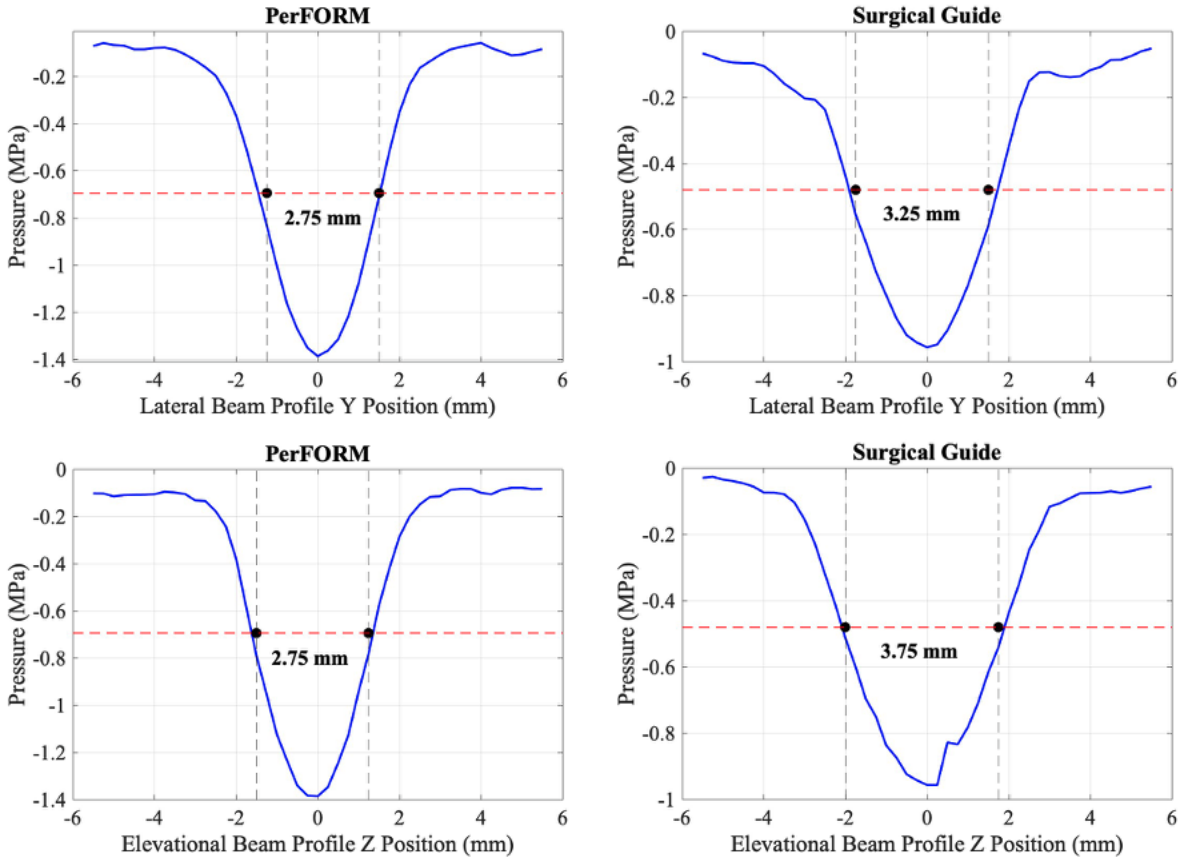

Figure 0-24. Lateral (top) and elevational (bottom) beam profiles for PerFORM and Surgical Guide. Beam widths were measured at the FWHM of the peak negative pressure and are indicated by red horizontal bars.

Figure 0-24 shows the lateral (Y) and elevational (Z) beam profiles for PerFORM and Surgical Guide, with beam widths calculated at the FWHM of the peak negative pressure. PerFORM exhibited a lateral and elevational beam width of 2.75 mm. In contrast, Surgical Guide produced broader beams, with a lateral width of 3.25 mm and an elevational width of 3.75 mm. These differences suggest greater beam spreading in Surgical Guide relative to the control material.

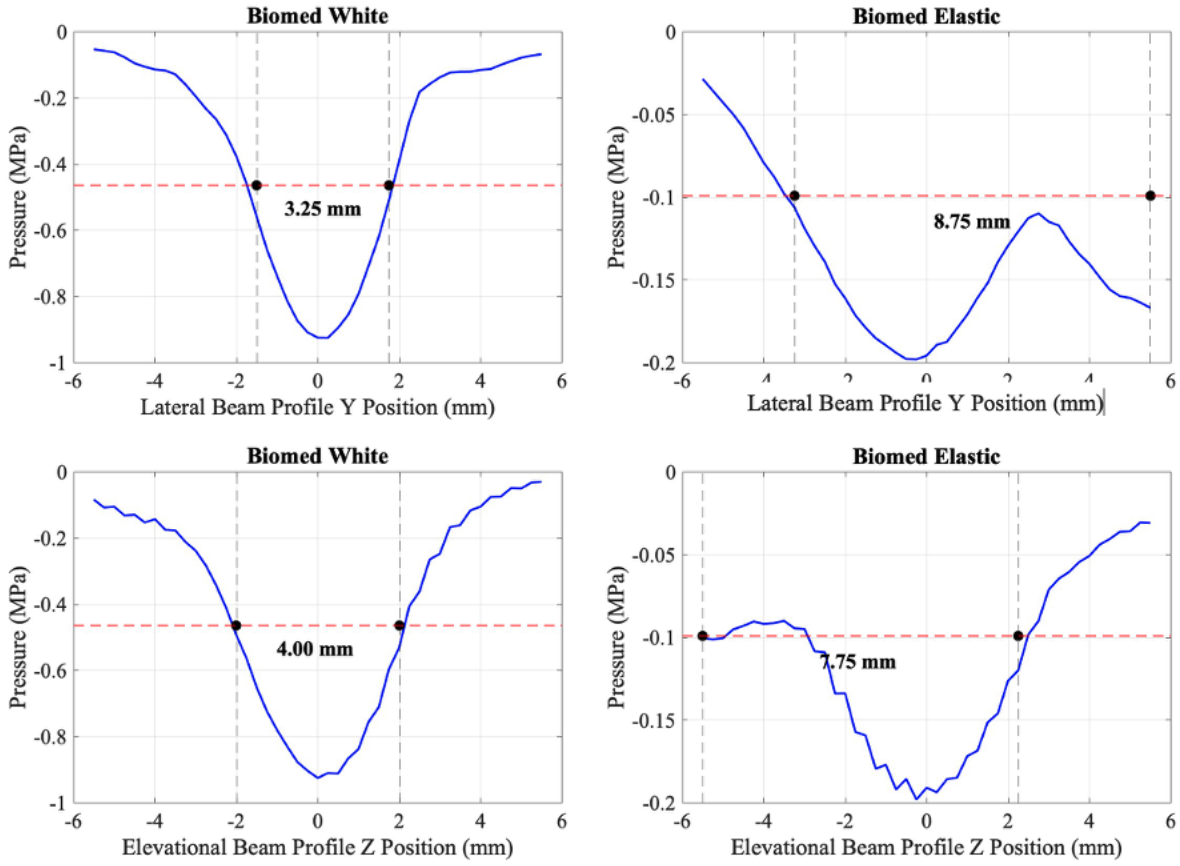

Figure 0-25. Lateral (top) and elevational (bottom) beam profiles for Biomed White and Biomed Elastic 50A. Beam widths were measured at the FWHM of the peak negative pressure and are indicated by red horizontal bars.

Figure 0-25 presents the lateral and elevational beam profiles for Biomed White and Biomed Elastic 50A, with beam widths determined at the FWHM of the peak negative pressure. Biomed White exhibited a lateral beam width of 3.25 mm and an elevational beam width of 4.00 mm. In comparison, Biomed Elastic 50A showed broader beam profiles, with a lateral width of 8.75 mm and an elevational width of 7.75 mm. These results indicate reduced focusing precision in Biomed Elastic 50A relative to the other tested materials.

I_{SPTA} values were calculated to assess the time-averaged acoustic intensity at the focus for each material. While pulse repetition frequency (PRF) is application-specific and can vary widely, a PRF of 100 Hz was used here as a representative estimate for calculation purposes. This does not reflect a worst-case scenario, which is important to consider during safety evaluations to ensure

that exposure limits are not exceeded under the most intensive operating conditions. As shown in **Table 14**, unscaled I_{SPTA} values ranged from 4.49 mW/cm² for PerFORM to 0.091 mW/cm² for Biomed Elastic 50A, reflecting differences in acoustic transmission efficiency. Surgical Guide and Biomed White exhibited intermediate I_{SPTA} values of 3.06 mW/cm² and 2.61 mW/cm², respectively. After scaling all waveforms to a peak negative pressure of -30 MPa, I_{SPTA} values increased proportionally across all materials, with PerFORM at 2075 mW/cm², Surgical Guide at 2938 mW/cm², Biomed White at 2333 mW/cm², and Biomed Elastic 50A at 2021 mW/cm².

Table 14: Summary of peak positive and peak negative pressures, along with acoustic intensity values computed from pressure waveform data across 2025 spatial points at the acoustic focus.

Symbols	Unit	PerFORM	Surgical Guide	Biomed White	Biomed Elastic 50A
p-	MPa	-1.39	-0.96	-0.92	-0.20
I_{SPPA}	W/cm^2	95.43	56.66	41.30	0.592
I_{SPTA}	mW/cm^2	4.49	3.06	2.61	0.091
$I_{SPPA(Scaled)}$	W/cm^2	44162	54413	42617	13148
$I_{SPTA(Scaled)}$	mW/cm^2	2075	2938	2333	2021
Lateral beam (y)	mm	2.75	3.25	3.25	8.75
Elevational beam (z)	mm	2.75	3.75	4.0	7.75

3.4 Discussion

This study applied a structured, risk-based framework to evaluate several 3D-printed materials for use in early-stage histotripsy transducers. The testing focused on three risks, biocompatibility, electrical safety, and acoustic performance, with the goal of identifying early constraints and informing future development pathways. While material-specific trends were observed, the broader contribution of this work lies in demonstrating a generalizable evaluation process that can be applied across different device configurations and materials.

Cytotoxicity testing using ISO 10993-5 extract methods showed that PerFORM did not meet requirements under either short-term (24h) or long-term (72h) conditions. In contrast, Surgical Guide and Biomed White showed no adverse outcomes under the same conditions, and no additional cytotoxicity was introduced after post-processing and sterilization according to manufacturer guidelines. Biomed Elastic 50A could not be sterilized using the autoclave method available and exhibited surface tackiness that retained particulate matter during handling. These observations indicate potential limitations in its compatibility with sterile processing or cleanroom environments. Further testing would be needed to assess its compatibility with alternative sterilization methods such as ethylene oxide. Incorporating cytotoxicity screening early in development allows for the identification of materials that may pose biological risks before they are integrated into device prototypes.

Electrical testing identified a ground bond failure at one of the amplifier box screws, indicating an incomplete connection between exposed conductive parts and the system ground. This condition can allow leakage currents to flow through unintended paths if there is no low-resistance route to ground. In clinical environments, such scenarios have the potential to cause electrical shock if stray currents pass through the patient or operator, particularly in cases involving conductive contact with skin or invasive probes. Identifying this issue during early testing underscores the importance of evaluating the entire electrical pathway, including external components, when assessing safety. As devices move toward clinical use, alignment with standards such as IEC 60601-1 provides a framework for verifying ground continuity and confirming that leakage current levels fall within defined thresholds.

Acoustic testing revealed variation in pressure transmission and beam profiles across materials. However, all lenses were designed using a fixed sound speed and were not adjusted to

account for material-specific acoustic properties. As a result, the focal position varied between materials, and absolute comparisons of focusing performance are limited. Despite this, intensity values were assessed against regulatory benchmarks. After scaling waveforms to a uniform peak negative pressure of -30 MPa, I_{SPPA} values still showed some variance, reflecting differences in pulse duration, while I_{SPTA} values converged, indicating similar time-averaged energy delivery across materials under normalized conditions. To perform histotripsy within the I_{spta} limits of 720 mW/cm^2 to avoid thermal effects, the PRF for these transducers would need to remain below 25-37 Hz depending on the transducer.

3.5 Conclusions and Future Work

This chapter outlined an example approach for evaluating rapid-prototyped materials for FUS devices through acoustic, electrical, and biocompatibility testing. These tests were selected based on high-priority risks identified through a risk-based framework developed earlier in the design process. Each test addressed an identified area of concern, biological compatibility, electrical continuity, and acoustic output, and was aligned with applicable regulatory standards, including ISO 10993 for biocompatibility, IEC 60601-1 for electrical safety, and IEC 62127-1 for acoustic measurements. The focus was not on material selection but on demonstrating a structured process for identifying safety and performance-related issues using accessible methods during early-stage development. This approach provides a model for how FUS prototypes can be evaluated in relation to clinical safety requirements before full system integration.

Future work will expand on the current evaluation framework by incorporating additional tests that address areas not covered in this study. Thermal output testing will assess the potential for unintended heating on the transducer surface by using thermocouples or infrared thermal imaging of components during operation. These measurements will be supported by computational

modeling to simulate heat generation and dissipation under various operating conditions, providing additional insight into temperature distributions and potential thermal hotspots. Results from both experimental and simulated data will be compared to relevant safety thresholds highlighted in the FDA guidance for diagnostic imaging. Hipot (high potential) testing will evaluate dielectric strength and insulation performance by applying a controlled high-voltage potential between conductive parts and ground using an electrical safety analyzer, in accordance with IEC 60601-1 requirements. This test is used to identify possible insulation breakdown and verify that the device can withstand elevated voltages without compromising electrical isolation. Drop testing, as part of mechanical durability evaluation, will be conducted to assess whether the device maintains structural integrity and safe operation after impact during handling or transport. This is directly related to electrical safety because mechanical damage can affect insulation, grounding, or internal wiring. Electrical testing should be performed after drop testing to verify continued compliance with IEC 60601-1. Additional acoustic measurements will include scanning along the axial axis to determine beam dimensions, using hydrophone-based focal mapping to identify focal length and assess alignment with imaging guidance with accordance to IEC 62127-1. Sterilization methods will also be evaluated for the fully assembled device using protocols such as autoclaving or ethylene oxide treatment, followed by post-sterilization inspection. These additional evaluations aim to build a more complete understanding of device safety and function in clinically relevant conditions.

3.7 References

[1] *ISO 14971:2019 Medical devices — Application of risk management to medical devices*.

[2] M. Bakaric, P. Miloro, A. Javaherian, B. T. Cox, B. E. Treeby, and M. D. Brown, "Measurement of the ultrasound attenuation and dispersion in 3D-printed photopolymer materials from 1 to 3.5 MHz," *J. Acoust. Soc. Am.*, vol. 150, no. 4, pp. 2798–2805, Oct. 2021, doi: 10.1121/10.0006668.

[3] *ISO 10993-5:2009 Biological evaluation of medical devices Part 5: Tests for in vitro cytotoxicity*, 2009.

[4] "IEC 60601-1:2024 SER." Accessed: Apr. 10, 2025. [Online]. Available: https://webstore.iec.ch/en/publication/2603

[5] "par.arisafety.com/ar_omnia_manual." Accessed: May 09, 2025. [Online]. Available: https://par.arisafety.com/ar_omnia_manual

[6] HIK Consulting, *3 Ways to Simplify Medical Device Testing*. [Online]. Available: https://www.hik-consulting.pl/files/3-Ways-to-Simplify-Medical-Device-Testing.pdf.

[7] "IEC 60601-2-62 IEC 60601-2-62:2013 Medical Electrical Equipment - Part 2-62: Particular Requirements for the Basic Safety and Essential Performance of High Intensity Therapeutic Ultrasound (HITU) Equipment," 2013.

[8] *IEC 62127-1 IEC 62127-1:2022 Ultrasonics - Hydrophones - Part 1: Measurement and characterization of medical ultrasonic fields*, 2022.

[9] Sheppard, Hannah. "Development of HIstotripsy Focused Ultrasound Devices Using Rapid Prototyping Methods." Virginia Tech, 2022.

[10] “ISO 10993-12:2021 Biological Evaluation of Medical Devices Part 12: Sample Preparation and Reference Materials,” 2021.

Chapter 4: Conclusions and Future Directions

Prototyping practices for FUS devices, particularly those developed for high-intensity applications such as histotripsy, are often carried out without early alignment to regulatory expectations. As a result, potential risks related to device performance, material compatibility, or safety may not be identified during the initial stages of development. This thesis introduced a risk-based evaluation framework intended to identify such risks early in the design process and to determine which could be addressed through modifications to device design. For risks that may not be mitigated through design alone, this work focused on assessing three critical aspects of device safety: biological compatibility, electrical safety, and acoustic output. Testing methods were selected to correspond with established regulatory standards and guidance documents, including ISO 10993 for biocompatibility, IEC 60601-1 for electrical safety, and IEC 62127-1 for acoustic characterization. The framework was applied to a set of 3D-printed materials used in rapid prototyping to evaluate their performance in relation to known risk categories when integrated into the device. The results showed that risks in one area may occur independently of others, reinforcing the importance of assessing multiple safety aspects in parallel. Structured evaluations conducted during early development can generate data relevant to regulatory standards and help identify factors that influence later stages of device design and integration.

This work focused on evaluating safety considerations at the material and component level. Future efforts could extend this framework to full-system prototypes by assessing how individual risk factors interact once components are integrated. Additional work may also involve aligning early testing with specific regulatory submission pathways, including documentation for preclinical studies. Applying this approach across a broader range of FUS applications could further clarify how treatment goals shape safety requirements. Continued refinement of testing

methods and integration of simulation tools may improve efficiency and reproducibility in early-stage device evaluation.

Appendix A. Example of Risk Assessment For FUS Devices

Hazard Type	Risk Description	Potential Harm(s)	Risk Rating	Guidelines/Standards to follow
Diagnostic	Limited imaging due to GI tract interference during targeting	May reduce targeting accuracy, impacting treatment efficacy	High	FDA Guidance Document for Diagnostic Imaging
Thermal	Overheating at the transducer's surface during treatment	Risk of thermal injury to tissue; may limit treatment duration or power	High	FDA Guidance Document for Diagnostic Imaging, IEC 60601-2-37, IEC 60601-2-62
Mechanical	Transducer or component detaches within GI tract	Mechanical failure could result in incomplete treatment or safety risk	Low	FDA Guidance Document for esophageal and tracheal prostheses
Mechanical	Perforation during insertion of the device	Potential for internal injury; raises concerns for minimally invasive access	High	FDA Guidance Document for esophageal and tracheal prostheses
Mechanical/Electrical	Device is cracked but is still used	Undetected cracks can lead to failure during treatment; affects durability	High	IEC 60601-1
Chemical	The material degrades due to exposure of high/low pH	Degradation may release harmful substances; limits compatibility with environments	Low	ISO 10993

Biological (Infection)	Inadequate sterilization or disinfection prior to insertion	Sterilization failures increase infection risk, undermining safety	High	ISO 11737
Biological (Material)	Transducer housing cause reaction in tissue	Adverse tissue reactions could limit material use or raise biocompatibility concerns	High	ISO 10993
Electrical Shock	Leakage or unintended contact with high-voltage	Shock risk compromises electrical safety; impacts compliance and trust	High	IEC 60601-1
Acoustic	Off-target acoustic injury to nearby tissue	Unintended damage may occur; limits use near sensitive tissues	High	FDA Guidance Document for Diagnostic Imaging, IEC 60601-2-37, IEC 60601-2-62
User Error	Operator misidentifies the target treatment zone	Human error can compromise targeting accuracy; impacts training and protocol development	Medium	Training and user manual
Mechanical (Assembly)	Improper assembly of imaging probe in transducer	Acoustic misalignment can lead to off targeting	Low	FDA Guidance Document for Diagnostic Imaging
Software/Control	Firmware or control software malfunction during treatment	Delivery of incorrect dose or parameters; loss of user control	High	IEC 62304

Thermal (Cooling Failure)	Active cooling system failure during high-power operation	Device shutdown or thermal injury at skin/probe interface	Medium	IEC 60601-2-37, IEC 60601-2-62

Appendix B. Acoustic Impedance and Sound Speed Matlab Code

```
function material_impedance_vals()

    % Sample names for the files
    names = {'BR1', 'BR2', 'BR3', 'BR4', 'BR5'};

    % Values for Biomed Convert mm to m
    thickness = [5.45, 5.47, 5.32, 5.49, 5.4] ./ 10^3;
    length = [30.17, 30.15, 30.21, 30.17, 30.21] ./ 10^3;
    width = [30.18, 30.09, 30.29, 30.13, 30.18] ./ 10^3;
    mass = [5.89,5.99,5.85,5.97,5.9] ./ 10^3;

    volume = length .* width .* thickness;
    density = mass ./ volume; % kg/m^3

    numSamples = numel(names);  % Use numel instead of length
    timeDif = zeros(1, numSamples); % Preallocate as a numerical array

    waterSpeed = 1484; % m/s, speed of sound in distilled water
    avgControl = 9.1e-08; % seconds (minimum peak of control wave form)

    % Load files of interest
    for i = 1:numSamples
        file_name = strcat(names{i}, '_3MHz_15mm_20V_.mat');

        if isfile(file_name)
            load(file_name, 'focusWave', 'timeValues');

            % Find the index of the minimum value in focusWave
            [~, ind_i] = min(focusWave);
            timeDif(i) = timeValues(ind_i);
        else
            % Provide a clear error message if the file is not found
            error('File %s does not exist.', file_name);
        end
    end

    % Calculate time differences and velocities
    timeDif = abs(timeDif - avgControl);
    velocity = (-waterSpeed .* thickness) ./ (waterSpeed .* timeDif - thickness); % m/s
    materialImp = velocity .* density ./ 1e6; % MRayls, (Rayl = kg/m^2/s)

    % Display the output without returning values to the command window
    disp('Velocity (m/s):');
```

```
    disp(velocity);

    disp('Material Impedance (MRayls):');
    disp(materialImp);

end
```

Appendix C. Attenuation Matlab Code

```
clear
close all
% Constants
% Convert thickness from mm to cm biomed resin white
thickness = [5.45, 5.47, 5.32, 5.49, 5.4] .* 0.1;
% Acoustic impedance of water
z1 = 1.48;
% Impedance values for each sample (excluding control)
z2 = [2.7853    2.8884 2.8657 2.8389 2.8854];
 % Input file names
names = {'Control','BR1', 'BR2', 'BR3', 'BR4', 'BR5'};

% Load files and analyze
numFiles = length(names);
peakAmplitudesMHz = zeros(1, numFiles); % To store peak amplitudes
frequencyData = cell(1, numFiles); % To store frequency data
magnitudeData = cell(1, numFiles); % To store magnitude data

% Loop through each file and plot individually for peak selection
for i = 1:numFiles
    file_name = strcat(names{i}, '_3MHz_15mm_20V_.mat');
    if isfile(file_name)
        load(file_name, 'focusWave', 'timeValues'); % Load data

        % Convert focusWave to pressure
        pressureWave = focusWave;

        % Adjusted Sampling Frequency based on timeValues
        Fs = 1 / mean(diff(timeValues)); % Calculate sampling frequency

        % Set up high-pass filter
        cutoffFreq = 1e6; % 1 MHz cutoff to remove low-frequency noise
        [b, a] = butter(2, cutoffFreq / (Fs / 2), 'high');

        % Apply high-pass filter
        filteredPressureWave = filtfilt(b, a, pressureWave);

        % Frequency domain conversion using FFT
        n = length(filteredPressureWave);
        f = (0:n-1) * (Fs / n); % Frequency range
        P = abs(fft(filteredPressureWave)) / n; % Normalized magnitude

        % Store data for combined plot
```

```
        frequencyData{i} = f(1:floor(n/2));
        magnitudeData{i} = P(1:floor(n/2));

        % Define the frequency range around 3 MHz (e.g., from 2.9 MHz to 3.5 MHz)
        freqRange = [1.1e6, 4e6];
        rangeIndices = find(frequencyData{i} >= freqRange(1) & frequencyData{i} <=
freqRange(2));

        % Find the index of the tallest peak within the range
        [~, selectedIndex] = max(magnitudeData{i}(rangeIndices));

        % Get the corresponding frequency and magnitude at the tallest peak
        selectedFreq = frequencyData{i}(rangeIndices(selectedIndex));
        peakAmplitudesMHz(i) = magnitudeData{i}(rangeIndices(selectedIndex));

        % Plot the frequency spectrum
        figure;
        plot(frequencyData{i}, magnitudeData{i});
        title(['Frequency Spectrum for ', names{i}]);
        xlabel('Frequency (Hz)');
        ylabel('Magnitude');
        xlim([0, 10e6]); % Limit x-axis if needed, e.g., to 10 MHz
        grid on;

        % Mark the tallest peak around chosen MHz
        hold on;
        plot(selectedFreq, peakAmplitudesMHz(i), 'ro', 'MarkerFaceColor', 'r');
        hold off;

    else
        error('File %s does not exist.', file_name);
    end
end

% Plot all frequency domain data on the same plot
figure;
hold on;
for i = 1:numFiles
    plot(frequencyData{i}, magnitudeData{i}, 'DisplayName', names{i});
end
hold off;
title('Frequency Domain Plot for All Samples');
xlabel('Frequency (Hz)');
ylabel('Magnitude');
xlim([0, 10e6]); % Limit x-axis if needed, e.g., to 10 MHz
legend('show'); % Display legend with names
```

```
grid on; % Optional: add grid for readability

% Extract control peak amplitude at chosen MHz
controlPeakAMHz = peakAmplitudesMHz(1);

% Calculate presRatio for the samples excluding control
presRatioMHz = peakAmplitudesMHz(2:end) / controlPeakAMHz;

% Calculate T for each sample using its specific impedance (excluding control)
T = (4 * z1 * z2) ./ (z1 + z2).^2;

% Calculate alpha based on T
alphaMHz = presRatioMHz ./ T;

% Units are in dB/(cm/MHz)
% Compute attenuation (multiplied by 2 because thickness was 0.5 cm but want it per dB/cm)
% attenuation3MHz = (20*log10(alpha3MHz).*2.*thickness)/Frequency;
attenuationMHz = (20./thickness).*(log10(alphaMHz));
% Display results
disp('Attenuation:');
disp(attenuationMHz);
```

Appendix D. Electrical Safety Analyzer Parameters

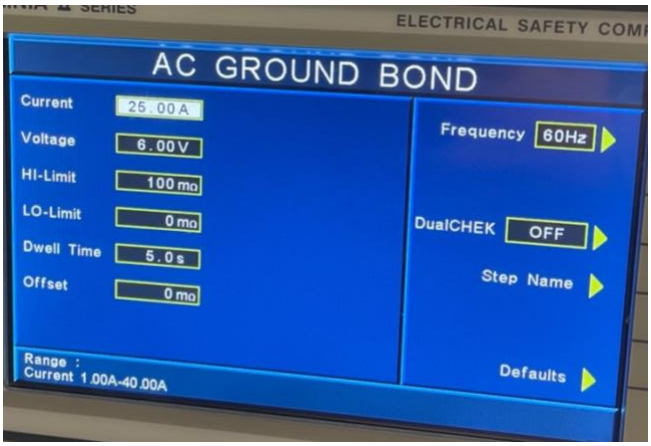

For Ground Bond test:

1.) Select AC Ground Bonde
2.) Set current to 25A and voltage to 6V
3.) Hi-limit = 100 mΩ and Lo-limit = 0 mΩ
4.) Dwell time = 5s and offset = 0

All leakage current tests have the same Leakage-Lo =0 uA, Voltage-Hi = 135V, Voltage-Lo = 130V, Dwell Time = 2s, and Delay Time = 2s. The measuring device should be IEC 60601 for all tests.
All the different Normal conditions and single fault conditions on the right-hand side of the screen can be adjusted accordingly to table 12 depending on what leakage test is being performed.
The leakage-Hi limit should be adjusted base on the type of test.
For earth leakage: Probe should go from Ground to Line
For enclosure one touch: Probe should go from Probe-Hi to Line
For enclosure two touch: Probe should go from Probe-Hi to Probe-Lo
For patient leakage: Probe should go from Probe-Hi to Line

Appendix E. I_{SPTA} and I_{SPPA} Matlab Code

```
clear; close all;

%% --- Load your grid-scan data (.mat must contain `gridWave` and `timeValues`)
load('/Volumes/Laura H Portable Drive/All the things/mat_files/BioElastic.mat');
%   gridWave    [N_rows × N_time] in MPa
%   timeValues  [1 × N_time]      in seconds

%% --- Physical constants & PRF
rho           = 1000;      % kg/m^3
c             = 1500;      % m/s
pressureFactor = 1e6;      % MPa → Pa
PRF           = 100;       % Hz

%% --- Preallocate arrays
[num_rows, ~] = size(gridWave);
ISPPA         = nan(num_rows,1);
ISPTA         = nan(num_rows,1);
pulseDur_us   = nan(num_rows,1);

%% --- Compute ISPPA & ISPTA per IEC 62127-1 for each row
for row = 1:num_rows
    % Convert pressure to Pa
    p_Pa   = gridWave(row,:) * pressureFactor;
    % Instantaneous intensity [W/m^2]
    instI  = p_Pa.^2 ./ (rho * c);

    % Cumulative energy and normalized envelope
    cumE   = cumtrapz(timeValues, p_Pa.^2);
    normE  = cumE ./ cumE(end);
```

```
    % Find 10% and 90% crossings
    i10    = find(normE >= 0.10, 1, 'first');
    i90    = find(normE >= 0.90, 1, 'first');

    % Pulse duration [s → μs]
    tau             = 1.25*(timeValues(i90) - timeValues(i10));
    pulseDur_us(row)  = tau * 1e6;

    % ISPPA = (1/τ) ∫_{t10}^{t90} instI(t) dt
    ISPPA(row) = trapz(timeValues(i10:i90), instI(i10:i90)) / tau;
    % ISPTA = ISPPA × τ × PRF
    ISPTA(row) = ISPPA(row) * tau * PRF;
end

%% --- Determine spatial-peak ISPPA
[ISPPA_spatial, idx_sp] = max(ISPPA);
ISPTA_spatial          = ISPTA(idx_sp);

%% --- Convert units for reporting and plotting
% ISPPA in W/cm^2
ISPPA_cm2    = ISPPA_spatial / 1e4;
% ISPTA in mW/cm^2
ISPTA_mW_cm2 = ISPTA_spatial / 1e4 * 1e3;

%% --- Display results
fprintf('\nIEC 62127-1 Acoustic Output Metrics (PRF = %d Hz)\n', PRF);
fprintf('Spatial-peak ISPPA: %.3f W/cm^2   (row %d)\n', ISPPA_cm2, idx_sp);
fprintf('Spatial-peak ISPTA: %.3f mW/cm^2  (row %d)\n\n', ISPTA_mW_cm2, idx_sp);

%% --- Extract the highest-ISPPA trace for plotting
p_Pa_sp    = gridWave(idx_sp,:) * pressureFactor;
instI_sp   = p_Pa_sp.^2 ./ (rho * c);
```

```
% Convert to W/cm^2
instI_sp_cm2 = instI_sp / 1e4;

% Recompute normalized envelope for shading
cumE_sp   = cumtrapz(timeValues, p_Pa_sp.^2);
normE_sp  = cumE_sp ./ cumE_sp(end);
i10_sp    = find(normE_sp >= 0.10, 1, 'first');
i90_sp    = find(normE_sp >= 0.90, 1, 'first');

% Times in µs
time_us    = timeValues * 1e6;
t10_sp_us  = timeValues(i10_sp) * 1e6;
t90_sp_us  = timeValues(i90_sp) * 1e6;
mask_sp    = time_us >= t10_sp_us & time_us <= t90_sp_us;

%% --- Plot intensity vs. time (W/cm^2) with shaded 10–90% region & ISPPA line
figure('Position',[200 200 600 400]);
plot(time_us, instI_sp_cm2, 'k-', 'LineWidth', 1.5);
hold on;

% Shade the 10–90% pulse region
hArea = area(time_us(mask_sp), instI_sp_cm2(mask_sp));
hArea.FaceColor   = [0.85 0.25 0.25];
hArea.EdgeColor   = 'none';
hArea.FaceAlpha   = 0.4;

% Dashed horizontal line at spatial-peak ISPPA (W/cm^2) with Times font, size 18
hY = yline(ISPPA_cm2, '--', sprintf('ISPPA = %.2f W/cm^2', ISPPA_cm2), ...
        'LineWidth', 4, ...
        'LabelHorizontalAlignment', 'right', ...
        'FontName', 'Times', ...
        'FontSize', 18);
```

```
% Zoom x-axis around the pulse
xlim([t10_sp_us-3, t90_sp_us+3]);

% Labels and formatting (Times, 18 pt)
xlabel('Time (\mus)',        'FontName', 'Times', 'FontSize', 18);
ylabel('Intensity (W/cm^2)', 'FontName', 'Times', 'FontSize', 18);
title('Biomed Elastic 50A')
set(gca, 'FontName', 'Times', 'FontSize', 18);

grid on;
box on;
```